FEDERAL UNIVERSITY OF ESPÍRITO SANTO

TECHNOLOGICAL CENTER

GRADUATE PROGRAM IN ELECTRICAL ENGINEERING

JOELSON DE CARVALHO ROCHA JÚNIOR

MASTER THESIS

---

# Design and Implementation of Electronic Architecture for Cloud Robotics and Human-Robot-Environment Interaction Strategy Applied to Smart Walker

---

VITÓRIA, ES, BRAZIL
SEPTEMBER, 2021

FEDERAL UNIVERSITY OF ESPÍRITO SANTO

MASTER DISSERTATION

---

# Design and Implementation of Electronic Architecture for Cloud Robotics and Human-Robot-Environment Interaction Strategy Applied to Smart Walker

---

*Author:*
Joelson de C. Rocha Júnior

*Advisor:*
Prof. Dr. Anselmo Frizera
*Co-Advisor:*
Prof. Dr. Ricardo C. Mello

*A dissertation submitted in fulfillment of the requirements for the degree of Master in Electrical Engineering*

*in the*

Electrical Engineering Department

VITÓRIA, ES, BRAZIL
DECEMBER, 2021

Ficha catalográfica disponibilizada pelo Sistema Integrado de Bibliotecas - SIBI/UFES e elaborada pelo autor

---

Rocha Júnior, Joelson de Carvalho, 1993-
R672d Design and implementation of electronic architecture for cloud robotics and human-robot-environment interaction strategy applied to smart walker / Joelson de Carvalho Rocha Júnior. - 2021.
98 f. : il.

Orientador: Anselmo Frizera Neto.
Coorientador: Ricardo Carminati de Mello.
Dissertação (Mestrado em Engenharia Elétrica) - Universidade Federal do Espírito Santo, Centro Tecnológico.

1. Engenharia Elétrica. 2. Robótica. 3. Computação em nuvem. 4. Sistemas homem-máquina. 5. Engenharia biomédica. I. Frizera Neto, Anselmo. II. de Mello, Ricardo Carminati. III. Universidade Federal do Espírito Santo. Centro Tecnológico. IV. Título.

CDU: 621.3

---

JOELSON DE CARVALHO ROCHA JÚNIOR

# Design and implementation of Electronic Architecture for Cloud Robotics and Human-Robot-Environment Interaction Strategy Applied to Smart Walker

*Dissertation was presented to the Graduate Program in Electrical Engineering of the Federal University of Espírito Santo as a partial requirement for the degree of Master in Electrical Engineering.*

Approved on December 13,2021.

Prof. Dr. Anselmo Frizera Neto - Advisor

Federal University of Espírito Santo

Prof. Dr. Ricardo C. Mello - Co-Advisor

Federal University of Espírito Santo

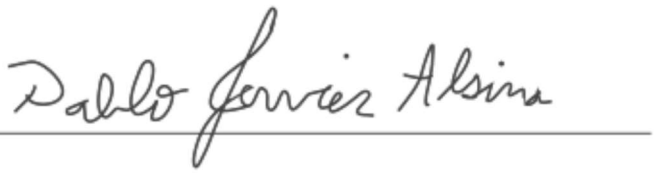

Prof. Dr. Pablo Javier Alsina

Federal University of Rio Grande do Norte - External Member

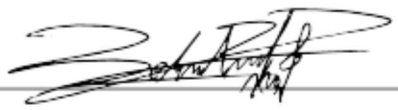

Prof. Dr. Camilo A. Rodriguez Diaz - Internal Member

Federal University of Espírito Santo

# *Resumo*

Técnicas para interação Humano-Robô-Ambiente permitem compartilhar o controle entre dispositivos assistivos, como andadores inteligentes, e seus usuários, levando em consideração a intenção de movimento humana e ambientes dinâmicos compostos por objetos e pessoas. Andadores inteligentes são robôs de serviço equipados com uma série de sensores e aturadores e têm finalidade de promover assistência à locomoção para pessoas com alguma limitação de movimento. A complexidade dos algoritmos utilizados para processar todos os dados aquisitados através dos sensores impulsionou pesquisadores a estudarem e explorarem conceitos de computação em nuvem, conhecidos como paradigmas de robótica em nuvem. Esta dissertação apresenta a modelagem e o devenvolvimento de uma arquitetura eletrônica para robótica em nuvem aplicada a um andador robótico. Através desta, o dispositivo robótico, chamado de UFES CloudWalker de agora em diante, é capaz de aquisitar e transferir dados para uma máquina virtual robusta que processa e converte-os em sinais de controle para os atuadores do robô. Esta dissertação de mestrado também apresenta um estudo dos andadores como dispositivos assistivos, bem como, estratégias de controle baseadas na interação entre humano, dispositivo robótico e ambiente. Mais a frente, desenvolvemos uma estratégia de interação robô-ambiente que foi avaliada em simulação e validada em ambiente real. Os resultados obtidos mostraram a confiabilidade dessa estratégia e nos levaram ao desenvolvimento de uma estratégia de interação humano-robô-ambiente no mesmo robô, através da detecção e rastreio das pernas do usuário. Finalmente, nós validamos esta estratégia no mundo real com obstáculos dinâmicos e estáticos. Os resultados mostram que o UFES CloudWalker é capaz de se adaptar às mudanças realizadas no ambiente e às intenções de movimento do usuário.

**Palavras-chave:** Interação Humano-robô-Ambiente. Dispositivos Assistivos. Andadores Inteligentes. Robótica em nuvem. UFES CloudWalker.

# *Abstract*

Techniques for Human-Robot-Environment Interaction allow sharing control between assistive devices, such as smart walkers, and its users by taking into account the human motion intention and dynamic environments composed of objects and people. Smart Walkers are service robots equipped with a series of sensors and actuators to provide locomotion assistance to impaired people. The complexity in the algorithms to process all the sensors data push researchers to study and explore concepts of cloud computing, called cloud robotic paradigms, in such platforms. This dissertation presents the design and development of an electronic architecture for cloud robotics applied to Smart Walker. Through this implementation, the robotic device, from now called UFES CloudWalker, is capable of acquiring and transferring data to a robust virtual machine which process and convert them in to control signals to the robot actuators. This Master's Thesis presents a study of smart walkers as assistive devices, as well as, control interaction strategies between the human, the robotic device and the environment. Moreover, we developed a robot environment interaction strategy which was evaluated in simulation and validated in real environment. The results showed the reliability of this strategy and boosted the development of a Human-Robot-Environment Interaction strategy in the same robotic device by adding information of the user's legs. Finally, we validated this strategy in real environment with static and dynamic obstacles. The results show that the UFES CloudWalker adapts its behaviour accordingly changes in the environment and the user motion intentions.

**Keywords:** Human-Robot-Environment Interaction. Assistive devices. Smart walkers. Cloud robotics. UFES CloudWalker.

# *Acknowledgements*

In this dissertation, this is the only page in Portuguese. This way, everyone who helped me will be capable of understanding my acknowledgments.

Primeiramente, agradeço a Deus por me acompanhar em todos os momentos de minha vida e sempre me dar discernimento para persistir mesmo em situações nas quais me vi em dúvida sobre o meu potencial.

Agradeço a minha família, em especial minha mãe Elka que, apesar de todas as adiversidades, me educou e sempre esteve por perto quando precisei. Agradeço a minha esposa Eloisa por estar comigo nessa jornada, pelas inúmeras vezes que sempre me motivou, mesmo eu não estando nada bem. Você tornou e torna os meus dias mais leves. Sua presença e a do nosso filho Luiz Filipe foram e são essenciais em minha vida. Amo vocês.

No âmbito acadêmico, agradeço ao meu orientador Prof. Dr. Anselmo Frizera Neto e ao meu coorientador Prof. Dr. Ricardo Carminati de Mello por todos questionamentos, críticas e conselhos que me deram durante o mestrado. Vocês me fizeram elevar o nível desse trabalho a um patamar que eu nem imaginava que era capaz de alcançar. Muitíssimo obrigado.

Gostaria também de extender os meus agradecimentos os meus colegas de laboratório e às amizades que construi nesse período. Em especial, aos meus colegas de trabalho que muitas vezes me ajudaram com questões técnicas, que melhoraram o *setup* dessa dissertação de mestrado, e sempre me motivaram a continuar dando o meu melhor. Meu imenso obrigado por sempre confiarem em mim e na minha capacidade.

# Summary

# List of Figures

# List of Tables

# List of Abbreviations

| | |
|---|---|
| **WHO** | **W**orld **H**ealth **O**rganization |
| **CP** | **C**erebral **P**alsy |
| **SW** | **S**mart**W**alker |
| **HRI** | **H**uman-**R**obot **I**nteraction |
| **REI** | **R**obot-**E**nvironment **I**nteraction |
| **HREI** | **H**uman-**R**obot-**E**nvironment **I**nteraction |
| **NTA** | **N**úcleo de **T**ecnologia **A**ssistiva |
| **UFES** | **U**niversidade **F**ederal do **E**spírito **S**anto |
| **LRF** | **L**aser **R**anger **F**inder |
| **IMU** | **I**nnertial **M**easurement **U**nit |
| **PC** | **P**ersonal **C**omputer |
| **GC** | **G**ait **C**adence |
| **LDD** | **L**eggs **D**ifference **D**istance |
| **FLC** | **F**ourier **L**inear **C**ombiner |
| **WFLC** | **W**eighted-Frequency **F**ourier **L**inear **C**ombiner |
| **IPSz** | **I**nter**P**ersonal-**S**ocial **z**one |
| **IPPz** | **I**nter**P**ersonal-**P**ublic **z**one |
| **FBG** | **f**iber **B**ragg **g**rating |
| **POF** | **P**olymer **O**ptical **F**iber |
| **VM** | **V**irtual **M**achine |
| **RGB** | **R**ed, **G**reen,**B**lue |
| **RGB-D** | **R**ed, **G**reen,**B**lue and **D**epth |
| **HRi** | **H**human-**R**obot **i**nterface |
| **UGV** | **U**nmanned **G**round **V**ehicle |
| **EKF** | **E**xtended **K**alman **F**ilter |
| **SFM** | **S**ocial **F**orce **M**odel |
| **LP** | **Lp** motion |
| **RL** | **R**einforcement **L**earning |

| | |
|---|---|
| **STS** | **s**it-**t**o-**s**tand |
| **EEG** | **E**lectro**e**ncephalo**g**raphy |
| **EMG** | **E**lectro**m**io**g**raphy |
| **ECG** | **E**lectrocardio**g**ram |
| **MIT** | **M**assachusetts **I**nstitute of **T**echnology |
| **JAIST** | **J**apan **A**dvanced **I**nstitute of **S**cience and **T**echnology |
| **FoV** | **F**ielf **o**f **V**iew |
| **PD** | **P**arkinson's **D**isease |
| **HMI** | **H**uman-**M**achine **I**nterface |
| **HCI** | **H**uman-**C**omputer **I**nterface |
| **BCI** | **B**rain-**C**omputer **I**nterface |
| **PUMA** | **P**rogrammable **U**niversal **M**achine for **A**ssembly |
| **OS** | **O**perational **S**ystem |
| **GPIO** | **g**eneral-textbfpurpose **i**nput/**o**utput |
| **SPI** | **S**erial **P**eripheral **I**nterface |
| **A/D** | **A**nalog to **D**igital |
| **ROS** | **R**obot **O**perating **S**ystem |
| **XMLRPC** | **XML**-**R**emote **P**rocedure **C**all |
| **NTP** | **N**etwork **T**ime **P**rotocol |
| **URDF** | **U**nified **R**obot **D**escription **F**ormat |
| **DWA** | **D**ynamic **W**indown **A**pproach |

*To my lovely wife Eloisa Lira, my son Luiz Filipe and my family.*

# Chapter 1

# Introduction

## 1.1 Motivation

According to a report of the World Health Organization (WHO) [1], the global population is expected to reach 9.7 billion in 2050. Two-thirds of this projected growth will be driven by current age structures. Low levels of fertility combined with increased longevity ensures that populations of all countries are growing older, resulting in a growth more than doubled in the people aged 65 population, while the number of children under five years is projected to remain relatively unchanged, between 2019 and 2050. In general people between the ages of 60-70 years start to present an accelerate decline rate in their walking speed [2].

Mobility is the most relevant physical ability that impacts directly people's life, whether in individual activities or in group [3]. This capability is reduced with aging, and neurological diseases such as cerebral palsy (CP) and stroke.

CP is a motor disorder caused by brain lesions that occur prenatally, or before two years of life. It affects directly the motor system causing spasticity, muscle hypertonia, muscle weakness and rigidity. Consecutively, individuals with CP, children and adults, present greater dependency, restricted social participation and a decreased quality of life [4].

Stroke is one of the major cause of adult disability and leads to difficulties in performing activities of daily living among victims [5]. Low limb spasticity is one prominent secondary consequence, which is directly related to further complicate stability control and has been estimated to occur in 13% - 12% of stroke survivors one year post-stroke [6].

The development of rehabilitation devices for people with mobility impairments is based on principles and capabilities of modern information technologies [7]. Rehabilitation based on the use of robot-assisted devices with biofeedback for motor training of upper and/or lower limbs still not popular in rehabilitation centers, but in a few years it could be a reality, especially in developing countries such as Brazil [8].

Currently, service and health robotics, more specifically for individuals with walking impairments, have became one of the main fields of study in robotics, allowing the researchers to develop assistive technologies to provide better quality of life through motor rehabilitation [9]. Motorized devices with intelligent control for passive-active robot-assisted therapy are widely used [10].

Advances in robotics allowed researchers to develop new generation of walkers, the Smart Walkers (SWs). Theses assistive devices present actuators and sensors providing assisted navigation, localization, obstacles detection and avoidance for people with disabilities [11]. In this context, one of the main challenges is how to share the control between the robotic platform, the user and the environment, composed of objects and even people [12].

Human-Robot Interaction (HRI) is one of the key points on the development of robotic devices that cohabit with humans, the so called service robots. To bring such devices to human lives, it is necessary to study and understand complex technologies from robot design, sensing, and control strategies to ensure safety and collaboration tasks efficiency [13]. Robot-Environment Interaction (REI) strategies allow the robot to collect information about static and dynamic objects, and also people within an environment, providing safe navigation through path planning techniques, as well as social interaction to its users [14].

Taking into account the benefits of both HRI and REI control strategies, the design and deployment of Human-Robot-Environment Interaction (HREI) strategies in service robots provide natural user interaction, as well as effective environment sensing and adaptation while maintaining safety requirements [15].

The necessity of real-time processing of the data produced by sensors incorporated in the SWs triggered the cloud robotics concepts deployment in such devices. Moreover, the robotic platform is seen as a set of services deployed on the

cloud, which can perform complex algorithms such as patterns recognition of camera frames, mapping and path planning, and communicate with another systems [16].

This dissertation presents and discusses technologies related to SWs: sensors, actuators and control strategies that provide adaptive behaviour to changes in the environment, user's movement intentions, or both simultaneously. This work also describes the design and implementation of electronic architecture of the new version of the UFES Smart Walker for cloud robotics, the UFES CloudWalker. This SW is capable of connecting bidirectionally with one or more servers, which process data and send back control signals in real time.

Moreover, the deployment of a REI control strategy based on mapping, localization and obstacles avoidance is evaluated in simulation and validations are conducted in real environment. Ultimately, a new HREI strategy based on the user's legs distance and the REI controller is deployed in the robotic device and validated in real environment. Results and further improvements are presented and discussed in the last chapter of this work.

## 1.2 Objectives

The main objective of this research is to develop and validate an HREI control strategy in the UFES CloudWalker. Through this approach, this service robot adapts its behaviour accordingly the environment constraints and the user's motion intentions. To accomplish this, the following specific objectives are proposed:

- To design and build the electronic architecture that enables to collect and process the data of the different sensors. It also allows communication with a server in local network and/or in the cloud. The processing can be done in the server or in both machines parallel.
- To develop, in simulation environment, and to validate, in real world, the mapping and localization, and the autonomous navigation modules for the UFES CloudWalker;
- To develop and to validate an HREI control strategy incorporating, in the UFES

CloudWalker, the autonomous navigation module and user's motion intentions signals to provide locomotion assistance and safety guidance simultaneously to its users.

## 1.3 Background of Smart Walkers in NTA

Smart Walkers have been the focus of research and development over the last decade at the Center for Assistive Technology (*Núcleo de Tecnologia Assistiva* - NTA) at UFES. Figure 1.1 illustrates an overview of the implementations conducted in our research group in the context of SWs.

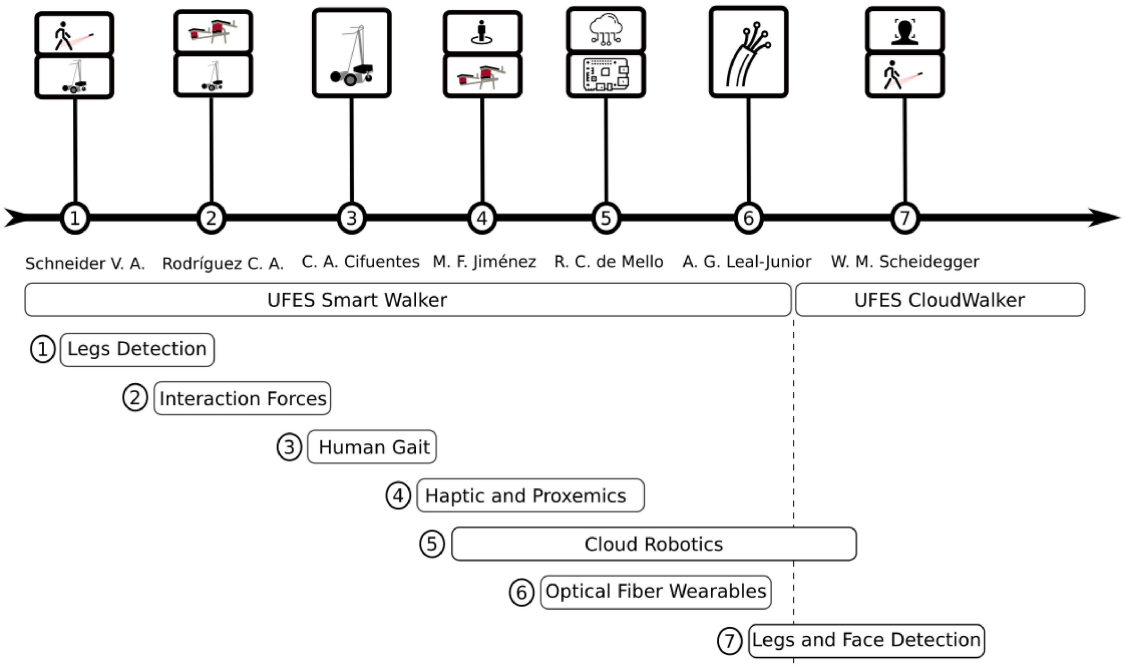


FIGURE 1.1: NTA background of Smart walkers development.

The first version of the UFES Smart Walker electronic architecture was developed by Schneider V. A. et al. [17] and Rodriguez C. A. et al. [18]. This robotic device is composed of two 3D force sensors MTA400 (FUTEK, US) [1], an embedded computer based on the PC/104-Plus (ADVANTECH, Taiwan)[2], one Laser Range Finder (LRF) sensor URG-04LX (HOKUYO AUTOMATIC CO., Japan) [3], two DC

[1] https://www.futek.com/store/multi-axis-sensors/triaxial/triaxial-load-cell-MTA400/FSH04139

[2] https://www.advantech.com.br/products/pc-104-i-o-modules/sub_1-2jklur

[3] https://www.hokuyo-aut.jp/search/single.php?serial=165

motors and one caster wheel, Figure 1.2. A Personal Computer (PC) was used for programming the real-time system, and to store data from the experiments.

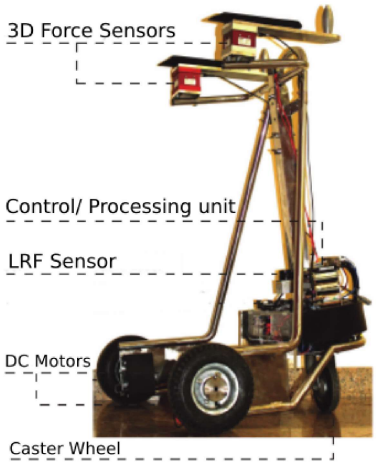


FIGURE 1.2: UFES SW First version. Source: [18].

In this opportunity, both researchers made the integration of all the sensors and actuators mentioned before with the PC/104-Plus. They also proposed and developed two HRI strategies: leg's detection module based on LRF sensor and user's interaction forces through the pair of 3D force sensors.

In [19], C. A. Cifuentes et al. developed a control strategy for walker-assisted locomotion based on the leg's detection module, a wearable Inertial Measurement Unit (IMU) sensor for human gait phase estimation and another attached to the UFES Smart Walker frame to predict the orientation error between the user and the robot platform.

M.F. Jiménez et al. made improvements in the UFES Smart Walker to promote HREI through a novel control strategy based on admittance controller with spatial modulation in virtual pre-defined paths [11, 20]. They allow the robotic device to infer the user's motion intention by using data from two 3D force sensors, Figure 1.3.A, located under the forearm supporting platforms. This SW also can provide, to its users, visual feedback through two LEDs (Figure 1.3.B). Once the user is being guided along the virtual path, a second LRF sensor RP LIDAR A1 (SLAMTEC, Shanghai)[4] acquires data from the environment and an obstacle detection algorithm process them to generate control signals when needed.

[4] https://www.slamtec.com/en/Lidar/A1

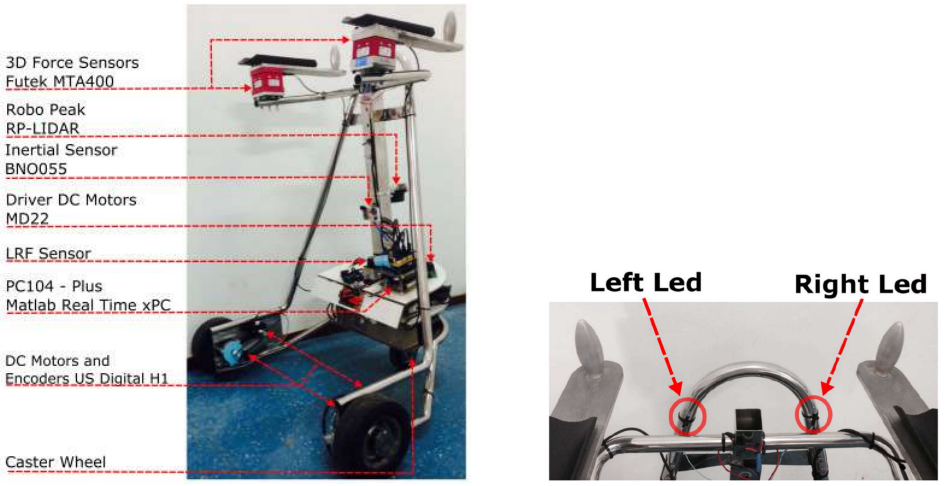


(A) (B)

FIGURE 1.3: (A) UFES SW improvements. (B) Left and Right LEDs position. Source: [20].

With the premise to allow social interaction in addition to locomotion empowering to the SW users, M. F. Jiménez et al. developed in [21] a new HREI control strategy based on proxemics, distance zones that human unconsciously maintains in social situations. Thus, this SW also takes into account social conventions and human behavior being capable of interact with both environment and the people around it.

The use of fiber Bragg gratings (FBGs) arrays in polymer optical fibers (POFs) to estimate the human gait cadence, floor vibration condition and human-robot interaction forces, and also oxygen saturation, breathing and heart rate were implemented in the UFES Smart Walker by A.G. Leal-Junior et al. [22, 23].

Advances in emergent control strategies and techniques applied to healthcare and service robots drove R.C. de Mello et al. to leverage the deployment of cloud robotics paradigms in the UFES Smart Walker, the CloudWalker architecture. This approach allows the SW to share data with remote machines which could store and also process the information parallelly, unlike the past implementations cited before.

The CloudWalker architecture dissociates the smart walker and its embedded system from the features it can offer (Figure 1.4). The centralization of services running on the cloud allows the data management and real-time processing faster than the traditional SW which have limited computational power [24].

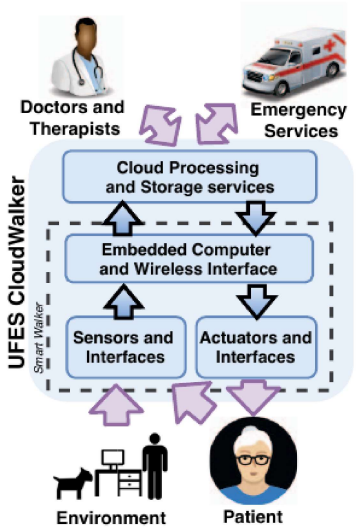


FIGURE 1.4: UFES CloudWalker overall architecture. Source: [24].

In order to make the communication possible between the UFES Smart Walker and the Virtual Machine (VM) possible, a Raspberry Pi 3 was used as a gateway. The sensor data is stored in it and the force signals are transmitted to the cloud, VM. A minimal version of the admittance-based controller presented in [20, 25] is implemented as a single service which takes the force signals as input and generates velocity commands to assist the user's locomotion, Figure 1.5.

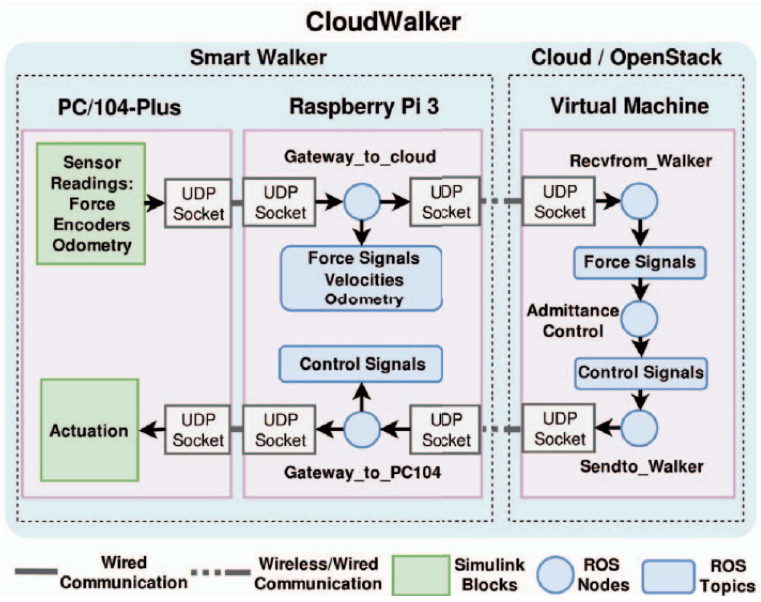


FIGURE 1.5: Network architecture between UFES Smart Walker and the Cloud. Source: [24].

In [26], R.C. de Mello et al. developed a cloud-based navigation service. The main difference here is that the robotic device, a UGV (Unmanned Ground Vehicle), is at the Colombian School of Engineering, Bogota D.C, Colombia configured to use of this service hosted at the remote cloud platform in Brazil. The robot collects and transfer to the cloud data from the environment and its odometry. The VM is responsible to send goals to the robot, read and process all the data received from it through Mapping and Localization services. Ultimately it sends back, to the robot, velocity commands (Figure 1.6).

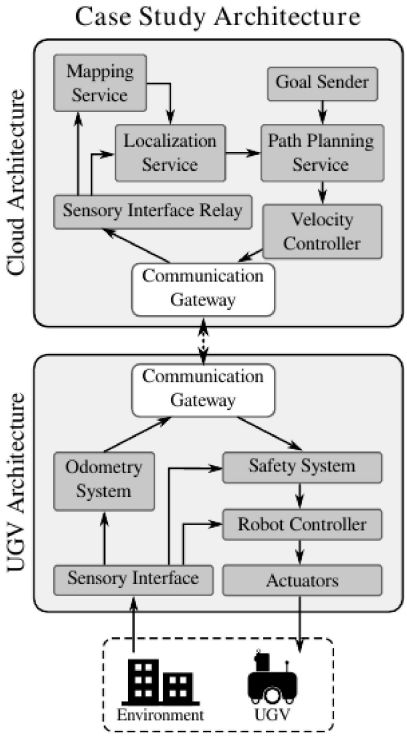


FIGURE 1.6: Overall architecture linking the UGV and the cloud-based navigation service. Source: [26].

W. M. Scheidegger et al. developed a novel multimodal cognitive interaction control strategy which leverages data from the user's legs and face orientation to command the SW displacement [27]. This work was done also in partnership with the Department of Biomedical Engineering of the Colombian School of Engineering, Bogota D.C, Colombia. This setup has two channels of cognitive interaction, the visual, through a Red, Green, Blue (RGB) camera, and the active ranging sensing by LRF sensor positioned to detect the user's legs, Figure 1.7.

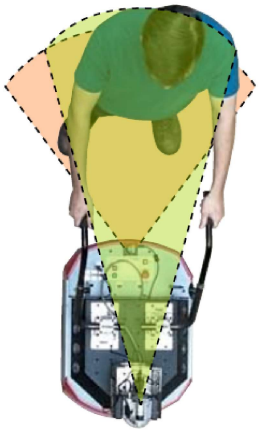

FIGURE 1.7: Visual and active ranging sensing channels. Source: [28].

Two services/modules are responsible to estimate the current user distance from the walker and face orientation. With these parameters a third service is used, the Follow-in-Front Controller. This service is responsible to generate and transfer linear and angular velocity to the robot low-level control system which makes the robotic device always be in front of the user.

The necessity to provide comfort, security, and rehabilitation to SWs users, advances in computing, and robotics triggered the emergence of new control strategies based on the interactions between the human, the robot, and the environment simultaneously. The following section discusses the most recently relevant technologies employed in SWs worldwide.

## 1.4 Justification

Literature reports that modern SWs have introduced HRI and HREI control strategies. These algorithms take into account data from several sensors, such as 2D and 3D LRFs [14], polymer optical fiber [22, 23], IMUs, RGB and RGB-D cameras [29, 30] aiming to estimate user's bio-mechanical and spatiotemporal parameters, motion intention and environment constraints. Due the high computational costs associated to the use of complex control strategies, some of these SWs have adopted cloud robotics paradigms as well as parallel processing optimizing their performance.

In Table 1.1, we present a summary of the current trends in the SW development. We used three main criteria to make it: the presence of motors for locomotion assistance (active), at least one shared control strategy, and the capacity of communicating with other machines in local network and potentially instantiated cloud systems (network-enabled).

| Reference | Walker/Author | Active | Shared Control Strategy | Network-Enabled |
|---|---|---|---|---|
| [31, 32] | Wachaja et al. | - | ✓ | - |
| [33] | i-walk | - | ✓ | ✓ |
| [34] | c-Walker | - | ✓ | ✓ |
| [35] | Zhao et al. | ✓ | ✓ | - |
| [36–38] | i-Walker | ✓ | ✓ | - |
| [39–41] | ISR-AIWALKER | ✓ | ✓ | - |
| [42–44] | MOBOT | ✓ | ✓ | - |
| [45–48] | ASBGo++ | ✓ | ✓ | - |
| [49–51] | CPWalker | ✓ | ✓ | ✓ |
| [52, 53] | AGoRA | ✓ | ✓ | ✓ |

TABLE 1.1: Summary of Related Work.

The robotic device developed by Wachaja et al. [31, 32] is a passive SW aimed to assist blind people with walking impairments needs. It was built by externally mounting sensors on an off-the-shelf walker, ensuring the faster user's adaptability to the new system.

This SW is equipped with two LRF sensors, a UTM-X002S (HOKUYO AUTOMATIC CO., Japan) [5] fixed and used to compute the ego-motion, and a UTM-30LX (HOKUYO AUTOMATIC CO., Japan)[6], continuously tilted up and down by a servo motor to create a 3D model of the environment. A computer is also used for data processing and one vibration motor attached to each handle for tactile feedback.

Its users also need to use a vibro-tactile belt which contains five vibration motors to warn about the objects in the environment closer them. This robotic device is able to communicate with a cloud server but only to update the map for navigation.

The i-walk lightweight rollator, presented in [33], is a passive SW which has not wheel encoders to track the motion of each wheel. It leverages the 2-D LRF sensor data readings to estimate its odometry and consecutively estimate its pose on a specific map. A Realsense D435i (INTEL, US) [7] depth camera is mounted in it to capture the user activity. The camera frames are processed in a Jetson TX2 (NVIDIA, US) [8] board to estimate the patient's 3D pose, action and gesture. This SW has also another features such as speech understanding, visual feedback to the user, and assisted navigation through speakerphone.

The c-walker [34] is a passive walker which provides shared strategies based on brakes control and shared steering, once it has stepper motors in each of the turning wheels and electromechanical brakes in the rear ones. Differently from the passive walkers cited before, this SW leverages data from both its egomotion sensors (wheel encoders and IMU) to estimate relative localization, front camera and a RFID reader to calculate absolute localization of markers (Qr codes and RFID tags), and a Kinect One (Microsoft,US) [9] sensor to estimate the 3D model of environment and reduce the robot position errors. The relative localization estimation is done locally, in the main board, through a multi-sensor data fusion technique, the Extended Kalman

[5] https://www.hokuyo-aut.jp/search/single.php?serial=170
[6] https://www.hokuyo-aut.jp/search/single.php?serial=169
[7] https://www.intelrealsense.com/depth-camera-d435i/
[8] https://developer.nvidia.com/embedded/jetson-tx2
[9] https://pt.wikipedia.org/wiki/Kinect

Filter (EKF) [54], while the other two algorithms are processed as services in a cloud VM.

This robotic device uses also the Social Force Model (SFM) [55] for path planning considering the pedestrians along the desired trajectory as attractive or repulsive forces to characterize their reluctance to stay too close to each other. It provides four different level of feedback to its users: mechanical (electrical brakes on the back wheels and stepper motors mounted on the front ones), haptic (vibrotactile bracelets), visual (screen) and acoustic (generation of 3D sounds).

Different approaches were conducted in active SWs. The SW developed by Zhao et al. [35] uses two hub motors and linear-pull brakes to provide guidance assistance for elderly people. This device infers user's motion intention through reinforcement learning (RL) techniques applied to lower limb gesture obtained from a 2D LRF and a infrared camera readings. An interesting feature of this SW is the autonomous mobility, which extracts time delay features from the user voice signal and send the robot to the user summoning through RL techniques for efficient sound source localization (SSL).

The i-Walker [36–38] is a modified 4-wheeled rollator with two hub motors integrated to the rear wheels and also two modified handlebars with brake handles and force measurement units (32 strain gauges mounted in 8 bridges). It leverages the handle bars force measurements to estimate spatiotemporal gait parameters of its users being capable of providing assistance in three different moments: active motor on climbs, active brake on descents, and active differential for asymmetric muscle compensation.

Aiming to replace the traditional force sensing technologies a vision-based approach was deployed in the ISR-AIWALKER [39]. This implementation is based on Leap Motion (Ultraleap, UK) [10], LP, sensors and springs, mounted on the walker handlebars. The data produced in this setup is used to generate fuzzy-logic commands to the low level controller and a safety gripping system which classifies if the user's gripping is adequate or inadequate for the SW use. The user's gait analysis system is equipped with an RGB camera and another LP sensor which are respectively used in the lower limbs, and the feet and heels strike detection modules.

[10] https://www.ultraleap.com/product/leap-motion-controller/

It also provides assisted navigation based on user intent adjustment [40, 41]. This approach uses Reinforcement Learning (RL) techniques to classify user's intentions, detects the environment constraints through a Microsoft Kinect One sensor and estimates the best route with a rapidly-exploring random tree-inspired algorithm.

The MOBOT [42–44] platform consists in the fusion of two robots: an active rollator robot for walking and a nurse-type for sit-to-stand (STS) assistance. It is equipped with Force, LRF, cameras, kinect sensors and microphones providing in total seven main functionalities to its user's: adaptability to the user (location, gestures, voice and postural stability), mapping, self-localization, autonomous mobility to approach the user from distance, physical assistance, autonomous parking and charging.

The ASBGo++ SW [45–48] was developed to provide safety, natural maneuverability and intelligent assistance in rehabilitation treatments for patients with ataxia. Equipped with two motorized wheels and multiple sensors, this robotic device acquires user's gait pattern data, movement intention and possibility of falls. The distance between the user and the SW is measured from IR sensors readings, a LRF sensor and RGB cameras are used for leg/foot tracking and upper body monitoring.

It presents four operating modes of this device: autonomous, manual, safety and remote control mode. The main difference between the ASBGo++ SW modes is that the autonomous mode just provides cognitive navigation assistance through a pre-defined path between the actual position and the target, while the manual mode uses mainly the handlebars as HRI strategy and the commands are defined on the interface by the users.

It is possible to combine the manual mode with the safety mode, in other words, while the user is guiding the SW a warning system is activated and it warns the user of a dangerous situation. Finally, remote control mode gives the possibility to the physiotherapists to monitor the user behavior, compensations, and reactions against changes in the user's speed and orientation.

The CPWalker combines SW and an active exoskeleton for assisted-therapies and complementary treatment for CP patients, once it is a disorder of posture and

movement due to a deficiency or lesion in immature brain [49–51]. This robotic platform is able to promote rehabilitation through a Multimodal Human-Robot Interaction interfaced by an Electroencephalographic (EEG) acquisition unit, Electromyography (EMG) system, IMUs and a LRF sensor to measure the human motion patterns.

The acquisition, processing and control are decentralized and shared between two embedded computers (PC-104) and one remote VM, as well as a tablet is used to allow the doctor the possibility to select the type of therapy, analyze the collected information and control the parameters in real time during the treatment execution.

The AGoRA Walker [52, 53] is a network-enabled SW which provides HREI through several interaction strategies. The HRI strategies implemented in this SW are recognition of user's interaction forces, navigation commands, presence and estimation of his gait parameters. Besides providing all these features, the robot also performs REI control strategies such as navigation system (mapping, autonomous localization and path planning), detection of surrounding people and path adaption due to social conventions.

The process of mapping is made off-line through the ROS gmapping package [56], which leverages the robot odometry and the LRF sensor readings about the environment to translate them as a grid-map image. This file is post-processed to reinforce the main constrains and characteristics of the environment. This SW can also be teleoperated remotely by a therapy supervisor who can also record session's data into a VM also.

The deployment of HREI control strategies on the cloud as services became a new trend in modern SWs. Due this fact, this master's thesis proposes an electronic architecture, the UFES CloudWalker, capable of providing lower limb rehabilitation to its users through modern HREI control strategies. Moreover, the development, implementation and validation of an autonomous guidance system centered in the user's motion intention will be covered in both simulation and real world environments.

## 1.5 Contributions

In this work, the author developed an electronic architecture to the new version of the UFES Smart Walker, the UFES CloudWalker. The integration of several sensors and the wheel motors of this robot, including the low and high level controllers was done, as well as the communication and parallel processing with another machine through local network.

Moreover, the author created the UFES Cloud Walker digital twin inside a simulation environment to boost the development of control strategies. This setup helped him to evaluate a REI controller as a first part of the deployment of an HREI control strategy in real world which takes into account the environment constraints and the user's movement intention

## 1.6 Publications

During the realization of this dissertation, the following paper was published and is directly linked to the work here presented:

- **Publication A: ROCHA-JUNIOR, J.C.**; MELLO, R.; BASTOS-FILHO, T.; FRIZERA-NETO, A. Development of Simulation Platform for Human-Robot-Environment Interface in the UFES CloudWalker. In: *2020 XXVII Congresso Brasileiro de Engenharia Biomédica (CBEB)*, SBEB, Vitória, 2020.

Lastly, the author participated in the other research work related to this dissertation; the main publication resulting from such activities is listed bellow:

- **Publication B:** L. B. P. Nascimento, **J. C. Rocha-Júnior**, V. G. Santos, D. S. Pereira, P. J. Alsina and A. Frizera-Neto. Fast and Safe Path Planning Method for an Autonomous Smart Walker. In: *2020 Latin American Robotics Symposium (LARS), 2020 Brazilian Symposium on Robotics (SBR) and 2020 Workshop on Robotics in Education (WRE)*, Natal, Brazil, 2020.

## 1.7 Dissertation Overview

This Dissertation is structured as follows. Chapter 2 introduces a study on mobility assistive devices, especially the conventional and smart walkers. Moreover,

it also discusses HREI and autonomous navigation (assisted guidance) strategies. Ultimately, concepts related to cloud robotics are clarified, as well as related work focused on assistive devices in the healthcare industry.

In Chapter 3, the robotic assistance architecture, UFES CloudWalker, and its digital twin are presented. Details of its subsystems to human and environment interaction control strategies, the proposed electronic architecture, the integration with remote VMs and the simulation environment setup are described.

In Chapter 4, the development of an Autonomous Navigation strategy is presented followed by evaluations made in simulation environment, and validations conducted in real world. This chapter ends with the analysis and discussion of the results from both scenarios, and preliminary conclusions.

Chapter 5 describes the implementation of a HREI strategy, which is a combination of two control strategies: the autonomous navigation, described in Chapter 4, and a HRI based on user's legs distance to the UFES CloudWalker. Results are discussed to validate this control strategy in real world, as well as, preliminary conclusions are conducted.

Finally, Chapter 6 summarizes this dissertation, presents the final remarks and future improvements.

# Chapter 2

# Theoretical Background

This Chapter presents concepts related to assistive devices for mobility, from traditional walkers variants to smart walkers and interaction control strategies (HRI, HREI and autonomous guidance). Ultimately, it discusses cloud robotics applications in healthcare focused in service robots.

## 2.1 Mobility Assistive devices

Assistive devices can offer support and assistance to people with different impairment conditions in terms of education, communication, leisure and mobility [57, 58]. In the mobility assistance context, these devices can be classified as alternative, when there is not locomotion capacity, or augmentative, when there is residual mobility. The selection of the best device to be used must be done after a physiotherapist clinical analysis, whose can choose and set the necessary adjustments in the equipment according to the user's needs [59].

In the universe of the alternative devices, wheelchairs (manual and motorized) and the special vehicles (e.g. scooters) have been developed and constantly improved (Figure 2.1). It is known that the continuous use of such devices may cause serious problems to the user (i.e. joint stiffness, skin ulcerations and deformities in the spinal cord). Due this, in cases when the users present a reminiscence level of locomotion capabilities, they are encouraged to adopt augmentative devices to empower their natural means of locomotion [60].

Several assistive devices emerged to empower, fully or partially, the residual capabilities of locomotion for daily activities. They were developed for people with gait impairments, being popular in elderly people, often with mobility difficulties

[60]. It is important to highlight that besides provide walk assistance these devices also prevent falls and reduce the impact in the user's lower limbs by supporting their weight partially. Augmentative devices are classified in two modalities: wearable, such as orthosis and prosthesis (Figure 2.2), and external, such as canes, crutches and walkers (Figure 2.3). Due the fact that walkers are the focus of this dissertation, we dedicate the following paragraphs to this topic.

(a) (b)

FIGURE 2.1: Examples of assistive devices: a) wheelchair; b) scooter

(a) (b) (c)

FIGURE 2.2: Wearable assistive devices: a) leg prosthesis; b) knee orthosis; c) leg calliper

(a) (b) (c)

FIGURE 2.3: External assistive devices: a) canes; b) crutches; c) walkers

Walkers are simple structures in which the users support their elbows or hands as a first step to initiate the gait. The main difference between the walker types is directly related to their ground contact configuration, being classified as: standard, reciprocal, two-wheeled, and rollators (Figure 2.4).


FIGURE 2.4: Walker types: a) standard; b) reciprocal; c) front-wheeled; d) rollator.

The standard walker, termed also as Zimmer frame or static frame, and the reciprocal walker, respectively Figure 2.4.a and Figure 2.4.b, are the best alternatives for people who can not support their own weight through an injured leg. The Zimmer requires a certain level of strength in the upper limbs to lift its frame to the next step [61], while the reciprocal mechanical structure allows the user to lift up and move one side to the frame at a time. These walking frames may be particularly useful for short-time rehabilitation.

Front-wheeled and rollator walkers are used when the patients have neither lower and upper body strength to walk. These walking aids also provide considerable support and a more fluid and natural gait in comparison with the standard [61].

The necessity to provide locomotion assistance in a more natural and comfortable manner, advances in the robotics and electronic fields allowed researchers to develop a new generation of walkers, called as Smart Walkers. These devices are able to measure the user's gait parameters and environment constraints through sensors, processing and communication units, and network capabilities for user's remote assessment [62]. Section 2.2 defines and discusses concepts related to the SWs development.

## 2.2 Smart Walkers

Besides providing physical support, the SWs can also offer sensory and cognitive assistance, and health monitoring to their users. At this point, the user can not only interact with it in a physical way but also cognitive, in other words, SWs have a certain level of intelligence to infer the human motion intention, allowing more natural gait to the user [20].

These devices are used also for extended features, such as gait and navigation assistance, sit-to-stand transfer, obstacle avoidance, and fall prevention [63]. Thus, SW are capable to increase the user's intimacy through control strategies that closes the loop between the human, robot and, in some cases, the environment also.

### 2.2.1 First development of Smart Walkers

Guido [64] is a SW developed by Haptica (Dublin, Ireland) aimed to blind people, developed from 1995 to 2001. The active and passive versions of it are depicted in Figures 2.5 and 2.6 respectively. In the active versions the robot had motorized traction and the speed was determined by user interaction with the force-sensitive handlebars unlike the passive, which did not have motorized traction, and a simpler user interface and a slightly lower cost of manufacture. These SWs were also equipped with sonar sensors and speakers. The commercial version of Guido launched in 2001 is depicted in Figure 2.7.


FIGURE 2.5: (a)-(c) Guido active versions 1995-1999. Source [64].

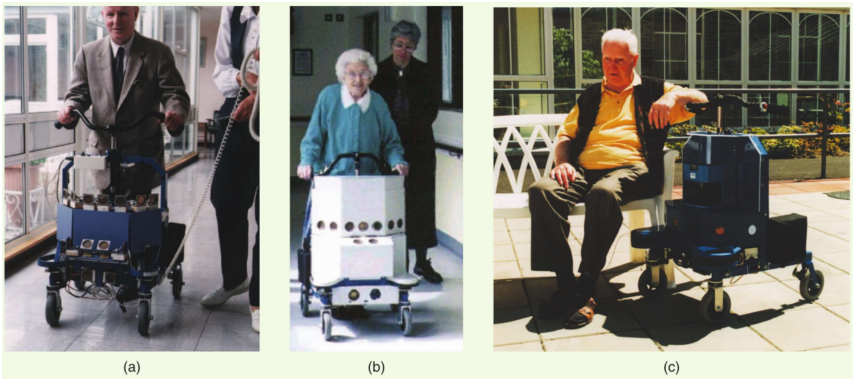


FIGURE 2.6: (a)-(c) Guido passive versions 1997-1999. Source [64].


FIGURE 2.7: Guido commercial version. Source [64].

The PAMM [65, 66] is another classical SW focused on mobility assistance to elderly and blind people referenced in several scientific papers. Its first version was built as a part of a doctoral thesis in Massachusetts Institute of Technology (MIT), back in 2002 . This passive SW has an adaptive shared control strategy based on the the user's motion intention, estimated through force sensors attached on its handlebars, and environment constraints. It also monitors the user's activity through a robust noninvasive electrocardiogram (ECG) based pulse monitor. Figure 2.8 shows the structure of the PAMM SW.

The JARoW (JAIST active robotic walker) [67], developed by researchers of the Japan Advanced Institute of Science and Techonology (JAIST). Its drive-train system is composed of three omni-directional wheels mounted underneath the base frame 120 degrees apart from each other. This allows the SW to move not only forward and backward but also to slide sideways and to perform rotations at the same spot.

FIGURE 2.8: PAMM Smart Walker structure. Source [66].

To estimate the user's lower limbs position, it is equipped with two sensor unities. Each sensor unity is basically an IR sensor mounted on the top of a servo motor, allowing to make readings in a certain Field of View (FoV) instead of a fixed point of interest.

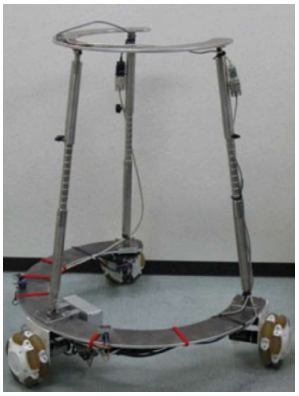

FIGURE 2.9: The JARoW SW prototype. Source [67].

The SIMBIOSIS SW [60, 68], developed by researchers of the Bioengineering Group of the Consejo Superior de Investigaciones Cientificas (CSIC) from the Universidad Politécnica de Madrid, Spain. This device is a passive walker with support for forearms. It presents two sensor subsystems designed for acquisition of gait parameters and characterization of the HRI during gait: the upper-body force interaction, based on two triaxial load cells installed under each of the forearm supporting platforms, and another based on ultrasonic sensors in which receivers are positioned on each user's legs and one emitter on the walker structure to measure the user's feet evolution during assisted gait. This SW is presented in Figure 2.10.

FIGURE 2.10: SIMBIOSIS Smart Walker structure. Source [68]

Developed by National Taiwan University researchers, the CAIROW SW presented in [69], Figure 2.11, uses a mini LRF sensor pointed to the user's legs to track the user's footsteps and to predict motion intention. This way, it keeps the same speed as the user: when he/she starts to walk, this SW begins also, and when he/she stops the robotic device will repeat this behaviour also. This mechanism is called "*Step-by-step*" which is its main feature.

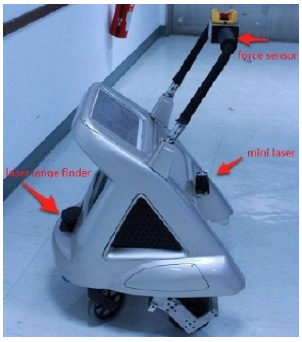


FIGURE 2.11: CAIROW Smart Walker overview. Source: [69]

This SW has two main modes: Autonomous and Rehabilitation. Through the Autonomous mode, it is possible to use the CAIROW as an mobile robot, sending it to a pre-defined localization where the user is near by, so it will performs navigation, localization and path planning to accomplish it. In the rehabilitation mode, the platform percepts both orientation, through flexiforce sensors installed on the handlebar, and user's intention of movement through the mini LRF sensor. It is also equipped with a touch interface in which the users can make an emergency call, emit alarms, chose a music to hear and select the velocity of the SW.

In the Subsection 2.2.2, we present some relevant works reported in the literature focused on the multimodal interaction strategies.

### 2.2.2 Current trends on SW: Multimodal Interaction strategies

The growing demand for closer cooperation and interaction between robots and humans boosted the design of more sophisticated robotic systems toward human-inspired solutions, as a road to replicate the human ability and flexibility in performing motor tasks. For such, the human-in-the-loop integration becomes one key element in which the Human-Robot Interaction (HRI) is an inherent element in the overall framework of Human-Robot interfaces (HRis) [70, 71].

Through the HRi, the information regarding cognitive processes is acquired and transmitted bidirectionally, supporting all the information flow that a smart system requires to perform its function [72]. In the literature, the terms human–machine interface (HMI), human-computer interface (HCI) and brain–computer interface (BCI) are related to this cognitive interaction between human-beings and robots [72].

In [73], an adaptive shared control strategy was developed into a SW providing auxiliary pelvic movement and ground walking. This robotic platform, Figure 2.12.A, leverages data from a force/torque sensor to support the user's body weight on walking, and a set of IMU sensors attached to the user body is used as input for the estimation of gait phase parameters, this way the robot is able to provide passive assistance when the user is walking, Figure 2.12.B.

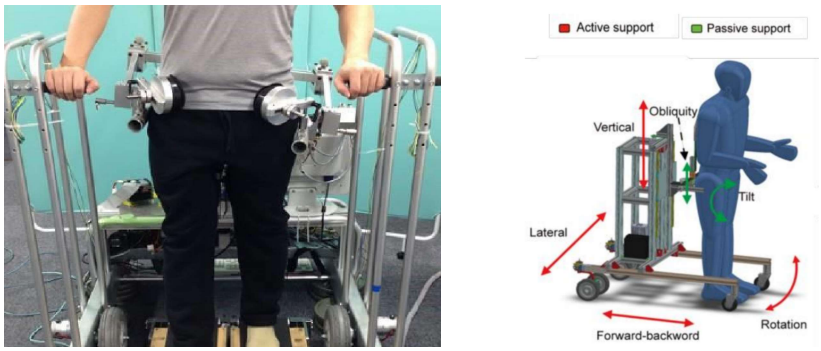


(A) (B)

FIGURE 2.12: (A) Robotic platform with pelvic and body weight support on walking. (B) Robotic walker overview. Source: [73].

Currently, besides having several HRis, modern SWs also use exteroceptive physical interfaces such as 2D and 3D LRF sensors [14], RGB and RGB-D cameras to detect environment constraints, as well as to provide context, guidance and social interaction to its users . The robotic platform is responsible to manage its mutual interactions with the human and the environment through shared control strategies. In the following paragraphs some examples of HREI control strategies applied into SWs are discussed.

Deployed in the AGoRA SW [52], Figure 2.13, the walker-environment sensory and social channel is responsible to store information such as obstacles and people near it. The people detection system complements the performance of a navigation system module enabling the walker with social acceptance and interaction skills.

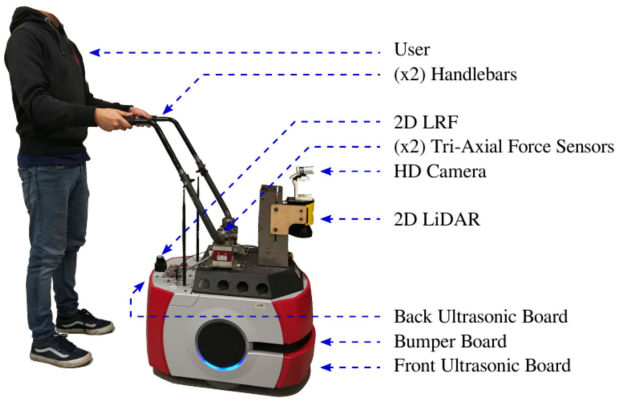


FIGURE 2.13: AGoRA SW overview. Source: [52].

This strategy combines data from two physical interfaces: a LRF sensor and a RGB camera. To minimize computational processing, this approach uses the laser readings to trigger the image processing by the camera frames. An overview of the methodology employed in this system is depicted in Figure 2.14.

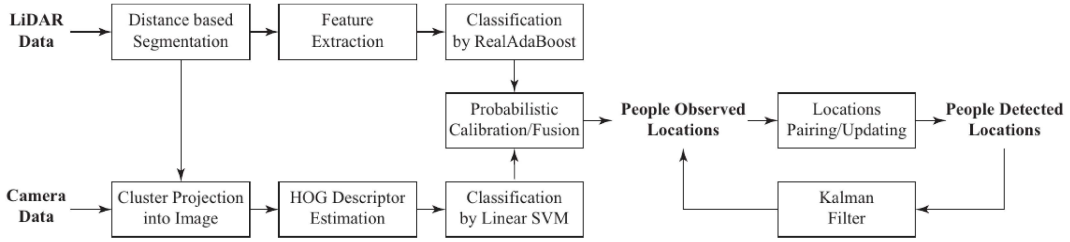


FIGURE 2.14: People detection module methodology. Source: [52]

The result of the distance based segmentation block is depicted in Figure 2.15.A. In the same way, these classification and the protection of these cluster into the output of the image processing is in the Figure 2.15.B. Thus, it is possible to see that three moving people were detected instead of four.

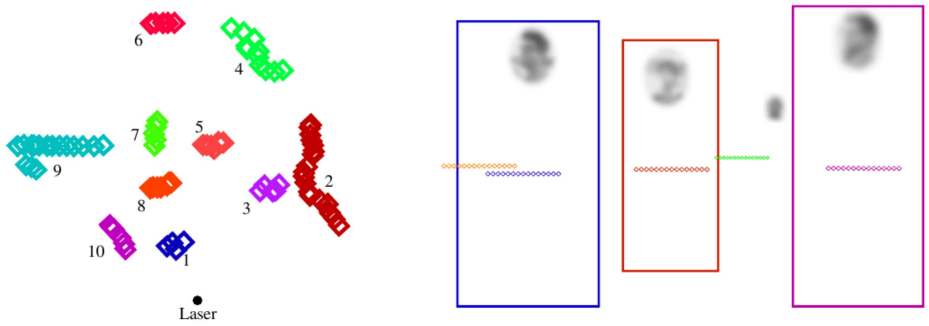


(A) (B)

FIGURE 2.15: (A) LRF clustering process output. (B) Detection of three people. Source: [52].

The emerging topic of social mapping deals with the challenge of robot's maneuvering in complex environments, where there is the presence of humans performing daily activities. This is accomplished through the embodiment of the rules of proxemics in robots [29, 74].

Jimenez et al. [21] developed an HREI controller based on proxemics for navigation in narrow spaces applied in the UFES Smart Walker. This approach is a combination of a admittance controller which converts the user's force/torque interaction signals in navigation commands and also modulates the user's haptic sense (more closer the SW is to the predefined path, more comfortable will be his guidance experience) in the path following task, and a obstacle detection module associated to proxemic rules which process the data from a LRF sensor aiming to classify objects and people.

The c-walker [34], Figure 2.16, is a rollator-like SW capable of providing lower limb rehabilitation and guidance. Three different cognitive channels (mechanical, haptic and acoustic) are used to provide guidance to its users in a reliable manner while sensing and processing information on user and environment.

Strategies for estimation and tracking of the SWs in mobile robots play a crucial role in the development directly related to autonomous navigation, harming, in

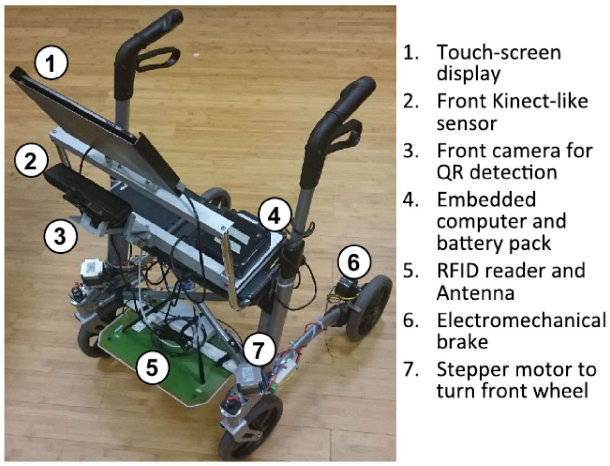


FIGURE 2.16: The c-walker SW. Source: [34].

some cases, the guidance performance. In an attempt to mitigate this possibility, an approach based on multi-sensor data fusion for position tracking was implemented in this SW.

This technique combines relative and absolute positions of the robot in the environment, Figure 2.17. The first one is achieved by integrating the information from the robot egomotion sensors (incremental encoders and gyroscopes) and have direct relationship on detection of an known object positioned in the navigation map. In contrast with it, the absolute tracking module detects real world inputs which are used to fix the localization of the robot in the navigation map. This SW has two absolute localization modules: based on markers (Front camera and RFID reader) and based on 3D model (Front Kinect).

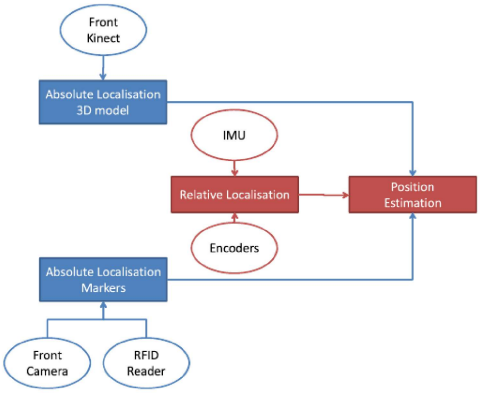


FIGURE 2.17: The c-walker localization tracking. Source: [34].

The RFID tags are positioned on the ground, and due the fact that they do not convey any information about the robot orientation, QR code markers are placed on the floor also. When this robotic device is moving across areas with nor QR visual markers and RFID tags, an remove service stored in the cloud is triggered. It performs an modified version of a Structure-from-Motion (SfM) from a Kinect device frame. Results of this process are depicted in Figure 2.18.A and 2.18.B.

(A) (B)

FIGURE 2.18: (A) Fabric hall 3D point cloud. (B) Estimated camera position in the scene. Source: [34].

Modern SWs have been empowering the user's guidance feature with HREI control strategies. The use of cloud robotics paradigms in these robotic devices allow to expand its functionalities through more sophisticated algorithms without compromise the SW processing unity. Next section discuss concepts related to cloud robotics and how the deployment of such, in service robots, has benefited the healthcare sector.

## 2.3 Cloud Robotics for Healthcare applications

Currently, the use of cloud computing to host an web based application or service became a popular practice. The computational resource availability and the system scalability are, without doubt, positive factors of this popularity [75]. This technology uses the service-drive business model [76], in which the infrastructure providers lend their resources in data centers as a utility to the service providers.

Virtualization is the technology responsible to build an abstraction layer between the host and the guest system. It helps in abstraction and isolation of multiple instances running on the same hardware within the cloud infrastructure [77]. The majority of the services hosted in the cloud environment are web based and easily

accessible through the internet. Some of othe popular cloud computing platforms are Amazon AWS [1], Windows Azure [2], Digital Ocean [3] and Google Cloud [4].

The cloud computing architecture is subdivided is four layers, Figure 2.19. The hardware layer is in which all the physical resources are managed, from power and cooling systems to switches, routers and servers. All these equipment are organized inside one or more data centers. The infrastructure, also known as the virtualization layer, creates a set of storage and computing resources by creating virtual machines in the physical sources. The platform layer consists of the operating systems and application frameworks. Ultimately, the application layer is at the highest level of abstraction, in which the cloud application is found. Cloud applications can have the auto-scaling feature enabled to ensure a better performance, availability and lower operating cost.

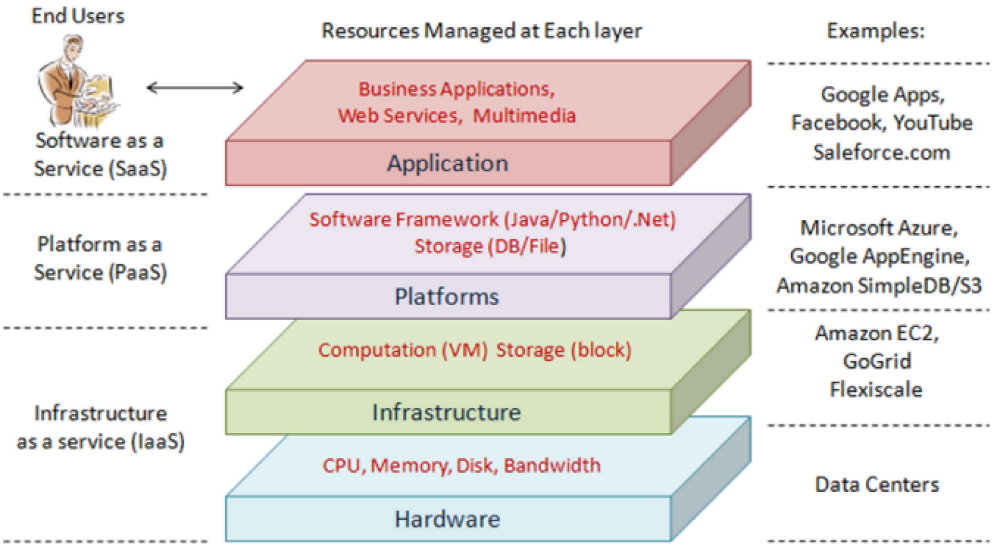


FIGURE 2.19: Cloud computing architecture. Source: [76].

Cloud robotics is an emerging field of robotics embedded in cloud computing, cloud storage and cloud networking [78]. Once the robotic device is connected to the cloud it is empowered by computational, storage and communication resources of modern data centers and shared services running on remote servers [79].

[1] https://aws.amazon.com/
[2] https://azure.microsoft.com/
[3] https://www.digitalocean.com/
[4] https://cloud.google.com/

Exploiting this topic, Bonaccorsi et al. [80] developed an cloud robotic system for the provisioning of assistive services for the promotion of active and healthy ageing. In it, the familiars and caregivers can monitor the seniors and the environments. The robot can act as a mediator between the users and the caregivers reminding him to take a medicine drug or detecting if the user is in a critical situation. Figure 2.20 shows how this platform allows the communication between the senior, the robot, the familiars and the caregivers.

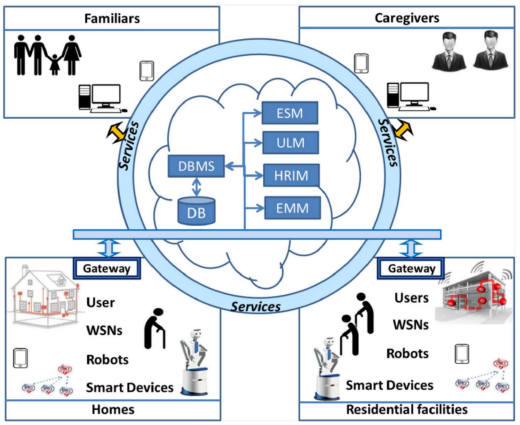


FIGURE 2.20: Overview of the cloud platform. Source: [80].

A similar approach was conducted in Fioring et al. [81], in which a personal health management service was deployed into the cloud and a service robot was used to mediate the communication between the caregiver and the senior. Figure 2.21 illustrates the relationship between the environment, user, robot and the cloud.

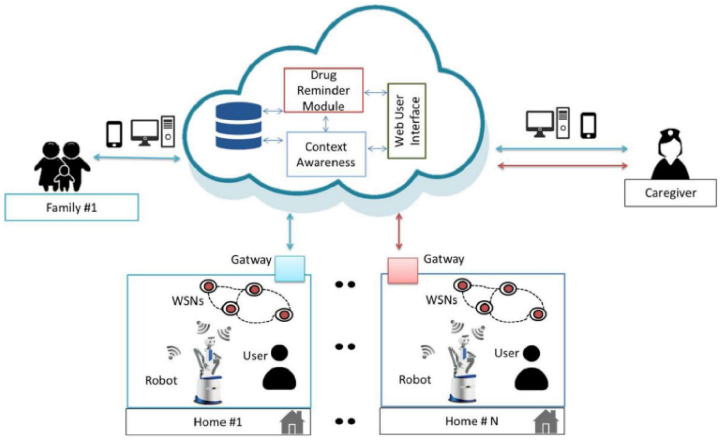


FIGURE 2.21: Environment, user, robot and sensor with cloud and Software as a Service (SaaS). Source: [81].

Radu et al. [82] built a cloud-based assistive system for HRI through an exoskeleton which basically stores the robotic device sensor's data for monitoring and historical purposes, and also training materials sent by an server on the cloud. Figure 2.22, shows the communication workflow of this application. This system is also equipped with an smartphone and a glasses with the function to inform the user about the exoskeleton status during operation.

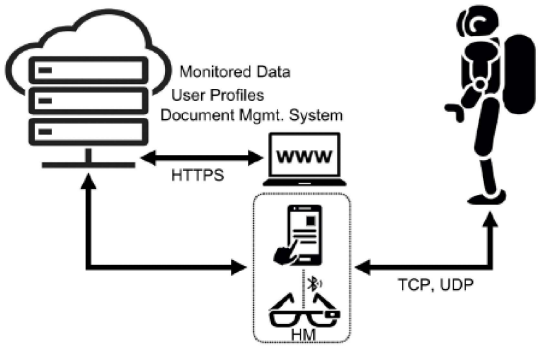


FIGURE 2.22: Assistive System for Human – Exoskeleton Interaction. Source: [82].

It is known that advances in cloud robotics increase the performance of service robot due the fact that the cloud has unlimited resources and can run 24 hours per day, this way all the developed services will always be running and the robot embedded computer will not be compromised [83]. Despite its attractiveness, cloud robotics requires a persistent connection to the cloud infrastructure, which is difficult to fully maintain, and other issues such as network traffic or reliability can result in higher latency, that affects the application real-time performance [84].

In face of all the concepts presented in this Chapter, this work envisions the integration of the UFES CloudWalker subsystems through a new electronic architecture, which also enables the communication with local VMs and the cloud. This process is described in Chapter 3. We present and discuss, in Chapter 4, the development, in simulation environment, and validation, in real world, of an autonomous navigation strategy based on mapping, localization, path planning and obstacles avoidance. Ultimately, we describe in Chapter 5, analyze and discuss the development and validation of a HREI strategy as a combination of the autonomous navigation strategy and the user's leg distance from this SW. In all the validations the processing is distributed between the robotic platform and a VM in local network.

# Chapter 3

# A Multimodal HRI Architecture

In this Chapter, we present an overview of the proposed robotic platform, the UFES CloudWalker. Details related to the hardware, software and networking topics, as well as, the integration with its subsystems for HREI strategies through the Robot Operating System (ROS) are described also.

## 3.1 UFES CloudWalker

The UFES CloudWalker [85] is a SW capable to promote rehabilitation and social interaction for people with motor disabilities. This robotic device presents a pair of triaxial force sensors MTA400 (FUTEK, US) [1], two LRF sensors URG-04LX (HOKUYO AUTOMATIC CO., Japan) [2] and RPLIDAR A3 (SLAMTEC, Shanghai) [3], a USB camera C920 (LOGITECH, Switzerland) [4], one depth camera Realsense D435i (INTEL, US) [5], one Inertial Measurement Unit BNO055 (ADAFRUIT, US) [6], two quadrature encoder H1-1024-IE-D (USDIGITAL, US) [7], two 24V Brushed DC Geared Motors (DOGA, Spain) [8] and one MD22 - 24V 5A dual H-bridge motor driver (DEVANTECH, UK) [9].

[1] https://www.futek.com/store/multi-axis-sensors/triaxial/triaxial-load-cell-MTA400/FSH04139
[2] https://www.hokuyo-aut.jp/search/single.php?serial=165
[3] http://www.slamtec.com/en/lidar/a3
[4] http://logitech.com/pt-br/product/hd-pro-webcam-c920
[5] https://www.intelrealsense.com/depth-camera-d435i
[6] https://learn.adafruit.com/adafruit-bno055-absolute-orientation-sensor/overview
[7] https://www.usdigital.com/products/encoders/incremental/shaft/H1
[8] https://www.dogaparts.es/en/dc-motors/
[9] https://www.robot-electronics.co.uk/md22-24v-5a-dual-h-bridge-motor-driver.html

The Figure 3.1 shows the UFES CloudWalker mechanical structure, which is built in aluminum and can be adjusted according the user's height, and all its electronic devices. The necessity to integrate the multiple sensors and actuators cited before, and to give capacity to attach new ones in the future were the main reasons to develop the UFES CloudWalker embedded system, called Walker_IC from now on.

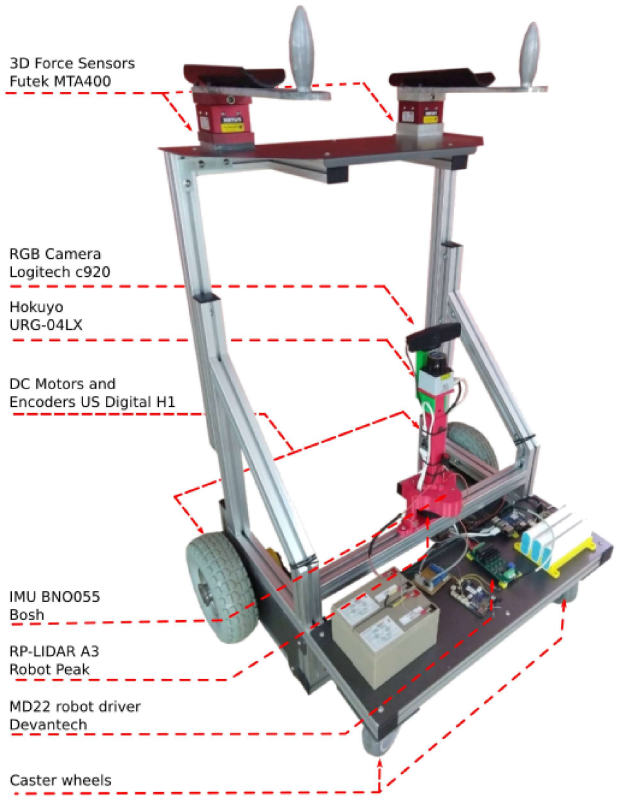


FIGURE 3.1: UFES CloudWalker mechanical structure and its electronic devices.

The Walker_IC was developed in a partnership between the NTA/UFES and the 2Solve Engenharia e Tecnologia [10]. This system was designed as a robotic version of the 2SToolsIC [11], a robust and flexible industrial computer for automation capable to acquire data from industrial sensors and cameras, to control processes and manage several equipment.

[10] http://www.2solve.com/
[11] http://www.2solve.com/tecnologias/computador-industrial.html

Its electronic architecture is basically structured in three parts: the Main, Extension and Communication boards. From bottom to top, the Main Board concentrates power supplies and is where the Raspberry Pi Compute Module 3+ (RASPBERRY PI, UK)[12], CM3+, 8GB version is attached and all its pins are distributed to the other two boards. The extension board is used to give new functionalities (Analog and Digital Input or Output) to general-purpose input/output (GPIO) pins from the CM3+. The Communication Board, is responsible to manage the USB, Ethernet and wireless connections as well as GPS, LORA and ZigBee.

Due the fact that the Communication and Main boards are common for both 2SToolsIC and the Walker_IC, the solution was to develop a new Extension Board. In Figure 3.2, we present an overview of this board in therms of communication protocols with the UFES CloudWalker electronic devices.

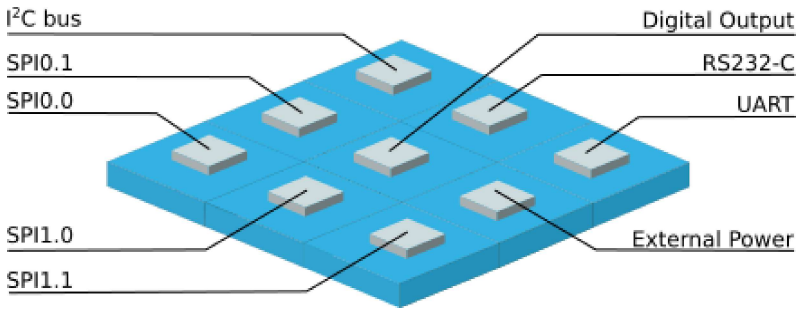


FIGURE 3.2: 2sToolsIC robotics extension board.

To acquire data from the pair of quadrature encoders we use the LS7366R-S [13], a 32-bit counter. The communication is done over Serial Peripheral Interface (SPI), devices SPI0.1 and SPI1.1. We use two MCP3208 [14], 8-channel 12-bit A/D converter, for the pair of triaxial force sensors data acquisition and for future integration of more eight possible analog devices to the robotic platform. The communication is also over SPI bus, devices SPI0.0 and SPI1.0.

The connection between the Hokuyo LRF sensor and the Walker_IC is done through the RS232-C connector, making possible the serial communication. This board has two $I^2C$ connectors, one for the MD22 dual H_bridge motor driver and another for expansion. The connection between the Walker_IC and the IMU BNO055 is done over the UART protocol.

[12] https://www.raspberrypi.org/products/compute-module-3-plus/
[13] https://lsicsi.com/datasheets/LS7366R.pdf
[14] http://ww1.microchip.com/downloads/en/DeviceDoc/21298e.pdf

We also leverage the two channels of digital output and external power, previous designed in the Main Board, and ultimately, to integrate the LRF sensor RPLIDAR A3, we use one the two USB connectors in the Communication Board.

Once all the physical connections between the Walker_IC and its electronic devices is presented, Section 3.2 presents all its embedded software development process: the Operating System configuration, the communication and time synchronization with another machine in local network, and the ROS framework used to develop all the integration with UFES CloudWalker subsystems for HREI strategies.

## 3.2 Networking and Software integration

The Operating System (OS) chosen for the Walker_IC was the Ubuntu Server 18.04 [15], a lite version of the Ubuntu 18.04 Desktop with less resources installed on it, which implies in more available space on memory. We chose this OS also due its full compatibility with the ROS framework due the fact that, in previous experiences with the Raspberry Pi OS Lite [16], the official OS suggested by the Raspberry Pi foundation [17], a Debian-based operating system, we had many problems with simple ROS package installation commands.

Figure 3.3 shows the physical connection between the Walker_IC and the Walker_PC, a second machine used to process the HREI strategies algorithms. Both Walker_IC and Walker_PC have static ip addresses over its Ethernet port respectively, 10.10.5.1 and 10.10.5.179. Due this the communication is possible only when both systems are on and connected with each other over the Ethernet cable.

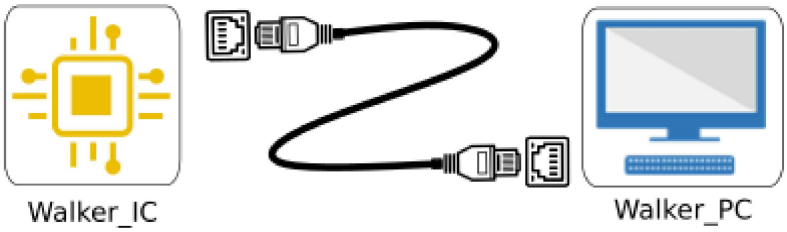


FIGURE 3.3: UFES CloudWalker Network Architecture.

[15] https://cdimage.ubuntu.com/releases/18.04/release/
[16] https://www.raspberrypi.com/software/operating-systems/
[17] https://www.raspberrypi.com/

Once both systems are in the same network, the time synchronization step begins through the NTP (Network Time Protocol). We use the chrony suite [18] to setup the Walker_PC as NTP server which answers the Walker_IC time synchronization requests and the parallel processing can be done between them with less possible error between their timestamps. The Walker_IC is responsible to acquire sensors data and for the UFES Cloud Walker traction, while the Walker_PC process them and return control signals to it.

The ROS [19] is a powerful and flexible framework which contains a collection of libraries and tools allowing collaborative development of robust and complex robots, and it supports several programming languages such as Python, C++ and Lisp.

This framework is described in [86] as a system that performs processes such as loading, monitoring and error handling by utilizing the virtualization layer between applications and distributed computing resources. We chose it, the Melodic Morenia distribution [20], to standardize the development of all the sensor and actuator drivers in the Walker_IC, as well as, the HREI and HRI control strategies in the Walker_PC.

In terms of terminology, ROS has some peculiarities and for the better understanding of this work some of them are described here. A ROS Master [21] is an entity that makes the message communication node-to-node possible. A ROS Node [22] refers to the smallest unity of processor running in ROS dedicated to an single purpose, for example: read a message encapsulated in a topic and print it in the screen. ROS messages [23] are objects that store data and are sent over ROS topics [24], name spaces in which the message is available when published by a node.

Figure 3.4 shows how the message communication happens between two nodes. For this purpose it is necessary that the ROS MASTER is instantiated in the machine, at least one node which publishes the information in an specific topic and another node that subscribes the same topic.

[18] https://chrony.tuxfamily.org/
[19] https://www.ros.org/
[20] http://wiki.ros.org/melodic
[21] http://wiki.ros.org/Master
[22] http://wiki.ros.org/Nodes
[23] http://wiki.ros.org/Messages
[24] http://wiki.ros.org/Topics

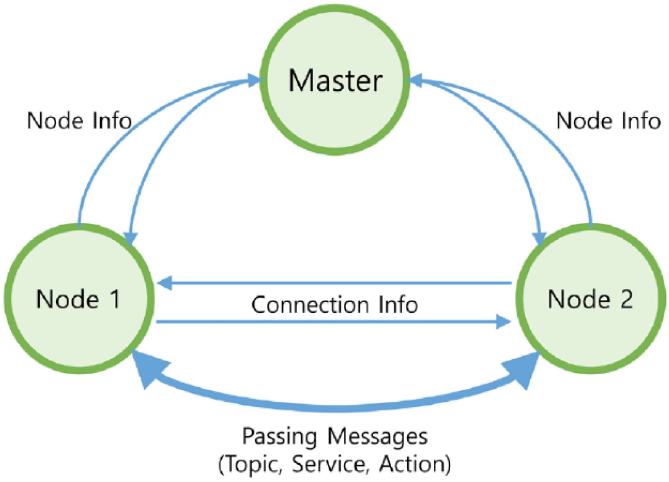


FIGURE 3.4: ROS message communication. Source: [86].

To make the Walker_IC and Walker_PC running as a single machine, we setup the master in the Walker_IC that communicates with the Walker_PC through XML-Remote Procedure Call (XMLRPC) [25], an HTTP-based protocol that does not maintain connectivity so the slave nodes can access only when they need to register their own information or request information of other nodes [86]. The ROS configuration between the Walker_PC and the Walker_IC is illustrated in Figure 3.5.

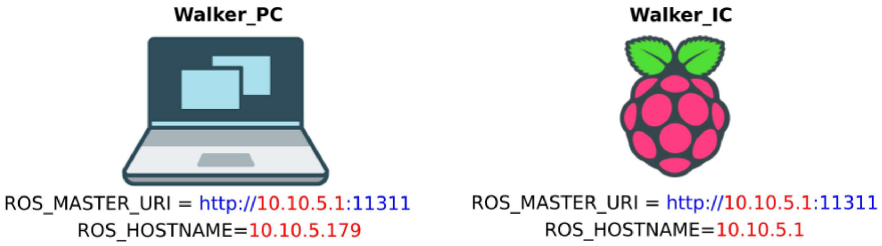


FIGURE 3.5: Network Connection between the Remote PC and Walker_IC through XMLRPC

To integrate the RPLIDAR A3 and Hokuyo LRF sensors we used their official ROS packages, respectively, rplidar_ros [26] and urg_node [27]. The Hokuyo data is available in the */scan* topic and the RPLIDAR A3 in the */rp_scan*. We developed the UFES CloudWalker low level controller, described in the appendix A.

[25] https://en.wikipedia.org/wiki/XML-RPC
[26] http://wiki.ros.org/rplidar
[27] http://wiki.ros.org/urg_node

The relative position is calculated through the odometry information from the wheels encoders and the IMU data, acquired by the *imu_ros_node* from the ros_imu_-bno055 [28] ROS node. We use the Robot_pose_ekf [29] ROS node, an implementation of the Extended Kalman Filter algorithm [87], to combine these data aiming to minimize position errors .

## 3.3 UFES CloudWalker Digital Twin

The UFES CloudWalker, Figure 3.6, is a SW able to promote rehabilitation and social interaction for people with motor impairments [28]. This robotic device presents a pair of triaxial force sensors, two LRF sensors, one RGB camera, one Inertial Measurement Unit and two quadrature encorders.

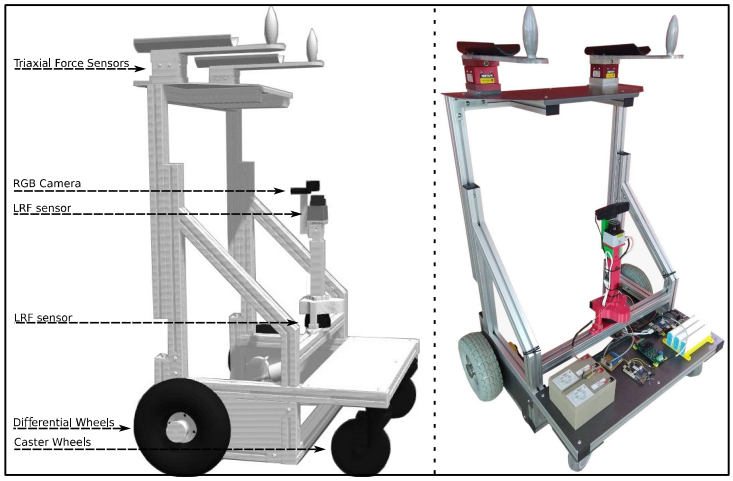


FIGURE 3.6: UFES CloudWalker digital twin (left) and real model (right)

We designed the UFES CloudWalker digital twin to speed up the development of a SLAM HREI, in which the physiotherapists will be capable of send one or multiple goals to guide the user during the therapy. We created it using the URDF [30] (Unified Robot Description Format) ROS package, in which, through an XML format, it is possible to describe the SW as a set of links and joints. Each joint has its own position and orientation represented by a frame. Due this, the *tf* [31] package was used in order to track information about the relationship of the robot frames.

[28] http://wiki.ros.org/ros_imu_bno055
[29] http://wiki.ros.org/robot_pose_ekf
[30] http://wiki.ros.org/urdf
[31] http://wiki.ros.org/tf

Through the Gazebo plugins [32], it was possible to give functionality to the Hokuyo LRF sensor and wheel actuators, and also to attach dynamic properties to the SW. For the map based HREI proposed, only the Hokuyo LRF sensor and the SW odometry data, provided by the relationship between the frames produced by the *tf* package, the *GPU laser* and *differential drive* gazebo plugins, were used.

To boost the development of HRI and HREI strategies, we envision a simulation environment inspired in a hospital floor plan. Thus, we leverage the *Gazebo* [33] simulator features to design a space similar to an hospital. The *rviz* [34] 3D visualization tool was used only for data visualization.

In Chapter 4, we describe the design, deployment and validation of an Autonomous Navigation strategy in the UFES CloudWalker. In it, we also discuss the results found in both environments, simulation and real world, and ultimately, we present our preliminary conclusions.

[32] http://gazebosim.org/tutorials/?tut=ros_plugins
[33] http://gazebosim.org/
[34] http://wiki.ros.org/rviz

# Chapter 4

# Design, Deployment and Validation of Autonomous Navigation Strategy

In this chapter, we detail both mapping and autonomous navigation strategies applied to the UFES CloudWalker. First, we describe the development and the results in simulation environment for the digital twin model of the UFES CloudWalker. After an evaluation and discussion of these results, we validate the proposed approaches in real environment with the robotic platform. Finally, preliminary conclusions of these experiments are presented.

## 4.1 Map Data Extraction and Robot Navigation Algorithms

Building maps is one of the fundamental tasks of mobile robots [56]. Researches often refers the mobile-robot mapping problem to as the simultaneous localization and mapping (SLAM) problem. The Rao-Blackwellized Particle Filters (RBPF), introduced by Murphy et al. [56], leverages the robot odometry measurements and the successive sensor environment observations to solve the SLAM problem with grid maps. Thus, we used the *slam_gmapping* [1] ROS node, an implementation of the RBPF technique, embedded in the ROS framework to create a 2-D occupancy grid map. Its hardware requirements are just a mobile robot that provides odometry data equipped with a LRF sensor.

[1] http://wiki.ros.org/gmapping

We used the Hokuyo LRF sensor and the UFES CloudWalker relative position estimations to achieve these requirements. Thus, we can manually control the SW around the environment, sending velocity commands, while this node collects all necessary information to generate the map.

The map representation consists of a grid-type grayscale image in which there are three different pixel tones: 255 are for navigable spaces, 0 means non-navigable, and 127 represents the unexplored ones. A sample of it is depicted in Figure 4.1. The *map_server* [2] node is used to save the map image and a *YAML* [3] file containing the map filename, the robot pose origin and the resolution (px/m) in which this image was generated.

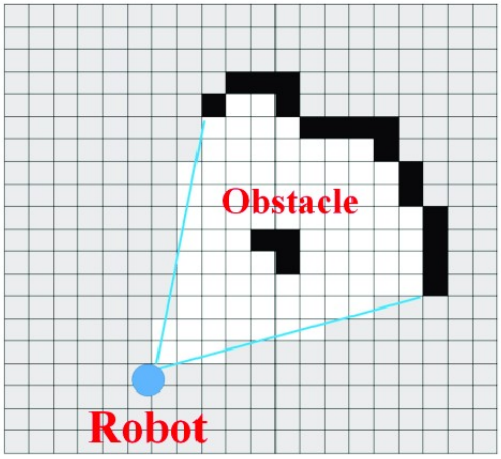


FIGURE 4.1: Example of an Occupancy grid map generated in the mapping process. Source: [88]

After the map building process, we leverage the *move_base* [4] ROS node, a standardized and configurable interface for mobile robot point-to-point navigation. Figure 4.2 illustrates the ROS Navigation Stack [5], which has the move_base node as its major component, optional provided and platform specific nodes.

The *map_server* is also responsible to load the map image and the *YAML* file, and to keep the map available in the */map* topic. We use the *amcl* [6] ROS node, a probabilistic localization system for a robot moving in 2-D based on the adaptive

[2] http://wiki.ros.org/map_server
[3] https://pt.wikipedia.org/wiki/YAML
[4] http://wiki.ros.org/move_base
[5] http://wiki.ros.org/navigation
[6] http://wiki.ros.org/amcl

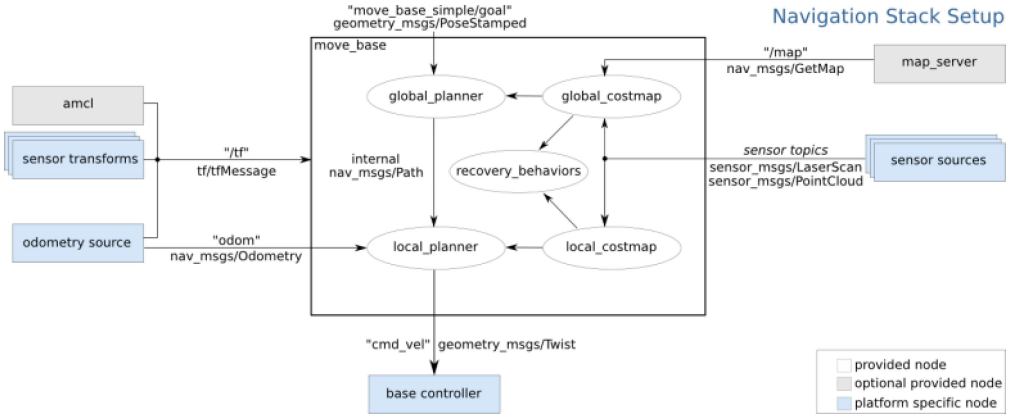


FIGURE 4.2: The move_base ros package workflow. Source: http://wiki.ros.org/move_base.

Monte Carlo Localization approach developed by F. Dellaert et al. [89]. It uses the LRF sensor readings to track the robot position in a known map.

We used the Dijkstra's algorithm [90] as the *global_planner* [7] of the *move_base* node. This algorithm finds the shortest path between the robot actual pose and the desired pose based on the *global_costmap*, the static representation of the map. In a smaller region around the robot, called as *local_costamp*[8], the previous path calculated by the global planner can be modified according the Hokuyo sensor readings while the robot is moving toward the desired pose avoiding collisions with unknown objects. This is only possible through the local_planner, based on the Dynamic Window Approach (DWA) [91].

The *inflation radius* is an important parameter for both planners. Through it, the robot will treat all paths that stay in the inflation radius surface or more away from obstacles as having equal obstacle cost, providing to the SW a safe path to navigate. Ultimately, given a plan to follow and the cost maps, the *base_local_planner* [9] sends velocity commands to the SW wheels through a kinematic trajectory for the robot to get from a start to a goal location.

To speed up the development and the adjustments of both strategies we used the UFES CloudWalker digital twin model reported in Section 3.3 and all the evaluations were conducted first in simulation environment. For the validation in real world, we used the UFES CloudWalker, described in Section 3.1. A remote machine, the

[7] http://wiki.ros.org/global_planner
[8] http://wiki.ros.org/dwa_local_planner
[9] http://wiki.ros.org/base_local_planner

Walker_PC, on the same local network of our robot was used to process all the high level controllers and we made all the trials in an office hall.

## 4.2 Experimental Protocols

The experimental procedures were conducted in two different scenarios. In the first one, supposing that the SW was brought or transferred to a new place, the environment is unknown and its task is to navigate autonomously while collecting environment data through the LRF sensor, and also to record it as occupancy grid map

The *teleop_twist_keyboard* [10] ROS node is used to send velocity commands to the robot. The map is generated six times and a dimensional comparison is conducted between 5 segments of the original environment. In the first five trials, the SW displacement were made in short paths attempting to visit the segments at least once, unlike the last trial, long ride around the map in which the robot visit each segment more than one time. We are interested to analyze the quality of the generated map in face of the robot detection frequency for each segment.

The trial maps and values are saved to evaluate the reliability of this approach. We developed the *FindSegments* [11] algorithm to finds each vertex in the generated map image and to measure the distance in pixels of the 5 segments through an implementation of the *Good Features to Track* algorithm developed by Jianbo Shi et al. [92] done in the OpenCV library [12]. The Equation 4.1 is used to convert the segment distance in pixels to meters, where the map_resolution = 0.05 meters/pixel.

$$Distance^{[m]} = distance^{[px]} map\_resolution^{[m/px]} \tag{4.1}$$

In the second scenario, we use the ROS Navigation Stack, explained in 4.1, to load the environment map and we sent a set of goals the SW, simulating a lower-limb guided therapy, conducted by the physiotherapist, through predefined paths.

[10] http://wiki.ros.org/teleop_twist_keyboard
[11] https://github.com/JoelsonCRJ/FindSegments
[12] https://opencv.org/

The evaluation of this approach was done by analyzing the SW pose error when it reaches each target, considering the unknown objects positioned between the targets. We use the Euclidean Distance to measure the position errors. Orientation are expressed in Euler angles unlike quaternions for simplicity.

## 4.3 Simulation Results and Discussion

This section presents the results in simulation environment of the mapping and localization, and autonomous navigation experiments. Evaluations about the errors from both approaches are conducted further.

### 4.3.1 Mapping and Localization

In this experiment we chose five different segments of the simulation environment to evaluate the generated map reliability, segments A to E. The SW displacement for each trial and one sample of the generated maps are exposed in Figure 4.3.

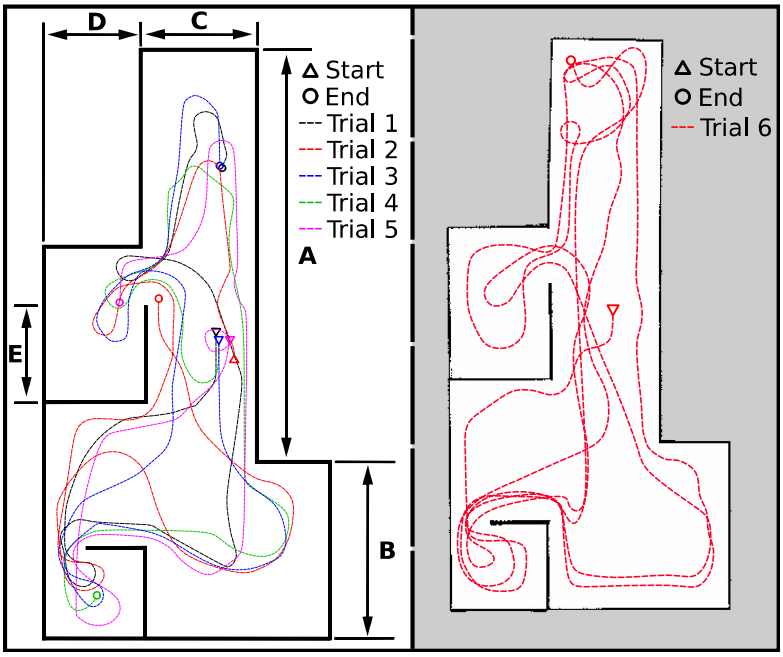


FIGURE 4.3: Simulation Environment (left), discriminating the measured wall segments and short paths performed in each of the first five trials, and; generated map sample (right), indicating the long path performed in trial 6

All the six maps were generated with the linear and angular velocities maximum values, respectively 0.5 m/s and 1 rad/s.The LRF Field of View (FoV) used in the experiments is 180° with 8 m of maximum range which is compatible with the Hokuyo installed in the UFES CloudWalker. This LRF sensor is attached to the SW's chassis at 70 cm high, same localisation of the used in the UFES CloudWalker, and the map resolution was 0.05 meters/pixel.

TABLE 4.1: Mapping and localization, short paths: results from trials 1 to 5 in simulation environment

| **Segment** | **Size(m)** | **Trials 1 to 5** | | | **Trial 1** | **Trial 2** | **Trial 3** | **Trial 4** | **Trial 5** |
|---|---|---|---|---|---|---|---|---|---|
| | | $\overline{Size}(m)$ | $\|\overline{error}\|$ (m) | $\overline{error}$ (%) | Size(m) | Size(m) | Size(m) | Size(m) | Size(m) |
| A | 19.026 | 18.131±0.419 | 0.897±0.378 | 3.653±1.375 | 18.500 | 17.550 | 18.550 | 17.901 | 18.152 |
| B | 7.974 | 7.530±0.076 | 0.444±0.068 | 5.355±1.006 | 7.500 | 7.450 | 7.500 | 7.650 | 7.550 |
| C | 5.359 | 4.911±0.065 | 0.448±0.058 | 8.356±1.085 | 4.950 | 4.850 | 4.850 | 5.000 | 4.906 |
| D | 4.741 | 4.511±0.041 | 0.231±0.037 | 4.864±0.781 | 4.550 | 4.550 | 4.451 | 4.501 | 4.500 |
| E | 4.500 | 4.380±0.126 | 0.120±0.112 | 2.658±2.500 | 4.451 | 4.500 | 4.200 | 4.451 | 4.300 |

Table 4.1 shows results from trials 1 to 5 for the mapping and localization experiment, in which the SW performed short paths to generate them, and in Table 4.2, the results from trial 6, in which we made a long ride with the robot around the environment.

TABLE 4.2: Mapping and localization, long path: results from trial 6

| **Segment** | **Size (m)** | **Trial 6** | | |
|---|---|---|---|---|
| | | Size (m) | $\|error\|$ (m) | $error$ (%) |
| A | 19.026 | 18.801 | 0.225 | 1.183 |
| B | 7.974 | 7.500 | 0.474 | 5.944 |
| C | 5.359 | 4.950 | 0.409 | 7.632 |
| D | 4.741 | 4.600 | 0.141 | 2.974 |
| E | 4.500 | 4.250 | 0.250 | 5.550 |

Due robot angular and linear velocities for all the trials were limited in 0.5 m/s and 1 rad/s, its rotation and displacement speeds, in relation to the segment, can be classified as fast or slow and may result in poor performance of LRF sensor [93]. In the learn process of the segment B, the robot made a rotation in a narrow corridor, which can be classified as a fast rotation and resulted in a high value of mean percentage error for this segment, 8.356%.

The standard deviation values of the mean percentage error shows the necessity to refine the robot pose estimation by adding new sensors to the robot, such as IMU and/or depth camera, and to use the Kalman Filter sensor fusion technique [94].

In trial 6, the robot performed a long path to map the environment. We compare its results, Table 4.2, with the results from trials 1 to 5, Table 4.1. This strategy reduces the error presented in the majority of the segments, except for segments B and E. These results indicates the necessity to conduct further studies in parameters of the *gmapping* ROS package such as the map_resolution, number of particle and update rate.

### 4.3.2 Autonomous Navigation and Obstacles Avoidance

In this experiment [13], four cylinders (radius = 0.5 m, length = 1.0 m) were positioned in strategic places along the robot target paths, stressing that the SW had no previous information about them in the generated map. We developed the *path_generator* ROS node which loads an *.csv* [14] file with the seven predefined targets, including the start and end desired robot positions, and send them to the SW by using the ROS *action_lib* [15]. The SW navigation behavior for all the four trials is exposed in the Figure 4.4.

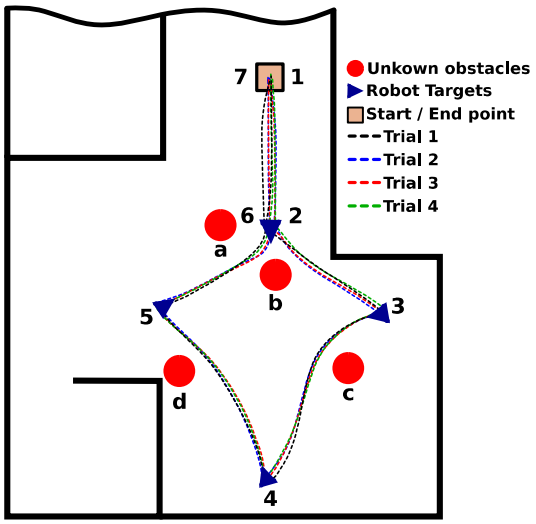


FIGURE 4.4: Results of all trials for the Navigation and obstacles avoidance experiment

The linear and angular velocities were limited in 0.5 m/s and $\pm 1$ rad/s respectively for all trials, and the *inflation_radius* was 0.5. The tolerance in meters for the controller in the x and y distance when achieving a goal, *xy_goal_tolerance*, was

[13] https://youtu.be/9eo07Nx4Lmo
[14] https://pt.wikipedia.org/wiki/Comma-separated_values
[15] http://wiki.ros.org/actionlib

setup to 0.10 m and the tolerance in radians for the controller in yaw/rotation when achieving its goal, *yaw_goal_tolerance*, was 0.05 radians.

TABLE 4.3: Results for Navigation and Obstacles Avoidance with Position (Euclidean distance) and Orientation (angular difference) errors

| Target | Target Pose [x, y, $\theta$] | Robot Pose [$\overline{x}, \overline{y}, \overline{\theta}$] | Position Error (m) | Orientation Error (rad) |
|---|---|---|---|---|
| 1 | [0.000, 0.000, 0.002] | - | - | - |
| 2 | [4.490, 0.000, 0.002] | [4.436±0.032, -0.031±0.029, 0.032±0.003] | 0.072±0.020 | 0.030±0.003 |
| 3 | [7.000, 3.000, -0.567] | [6.939±0.034, 2.977±0.019, -0.544±0.016] | 0.071±0.027 | 0.024±0.016 |
| 4 | [12.000, 0.000, -2.574] | [12.074±0.023, 0.103±0.036, -2.534±0.029] | 0.113±0.025 | 0.044±0.023 |
| 5 | [7.000, -3.000, 2.294] | [7.005±0.012, -2.929±0.031, 2.334±0.013] | 0.071±0.031 | 0.039±0.013 |
| 6 | [4.490, 0.000, 3.141] | [4.511±0.024, -0.112±0.037, 3.115±0.016] | 0.118±0.033 | 0.027±0.016 |
| 7 | [0.000, 0.000, 3.141] | [0.060±0.023, -0.003±0.012, 3.112±0.018] | 0.062±0.022 | 0.029±0.018 |

The mean value ($0.31 \pm 0.04$ m/s) of the trials linear velocities performed by the simulated SW were less than the 0.5 m/s, typical gait speed for an usual pace in elderly without any gait disorder [11].

The SW reached all the targets without any collisions, which means that the robot is able to interact with new objects in the environment. It's important to highlight the influence of the *inflation_radius* parameter for the safe paths generation task. If this value was higher than 1 m, the SW won't create a path between cylinders *a* and *b*, instead it will moves outside them to reach target 6.

The targets, SW pose, the Euclidean distance between the destination point and the place where the robot stopped and the orientation error for all trials are exposed in Table 4.3. Due the start point of the robot is the same that target 1, values of the robot pose as well its errors were removed.

All the position errors were less than the xy_goal_tolerance, 0.10m, except in the targets 4 and 6, in which the obstacles are closer to them. Ultimately, the orientation errors from all the segments were less than the yaw_goal_tolerance, 0.05 radians. These results could be influenced by the inaccurate SLAM strategy, evaluated in the previous experiment.

## 4.4 Validation Results and Discussion

This section describes the validation of mapping and autonomous navigation strategies, developed in simulation environment, in a real environment. It is necessary to highlight that unlike the UFES CloudWalker digital twin, presented in

Section 3.3, that uses the gazebo plugins as abstraction of its actuators and sensors, in the UFES CloudWalker, described in Section 3.1, we made some adjustments in the high level algorithms to met its electronic devices limitations.

### 4.4.1 Mapping and Localization

To validate the mapping and localization approach in real world, five walls of a lobby were chosen to evaluate the generated map reliability, Figure 4.5. A measuring tape was used to estimate their length.

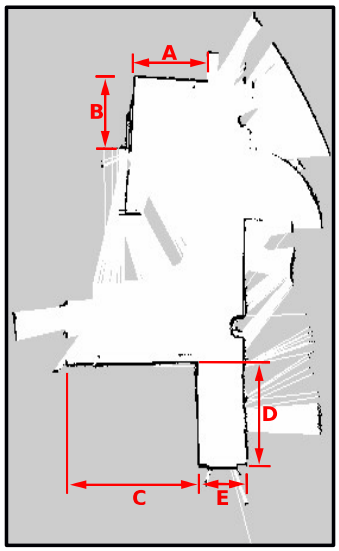


FIGURE 4.5: Segments selected for Mapping and localization experiment

All the six maps were generated with the linear and angular velocities limited to 0.25 m/s and 0.25 rad/s respectively. The Hokuyo LRF sensor was positioned 70cm above the ground with a FoV of 180° and 8 m of maximum range. All the generated maps and the respectively SW displacement are exposed in Figure 4.6.

Table 4.4 shows results from trials 1 to 5 for the mapping and localization experiment, in which the SW performed a short path, and in Table 4.5, the results from trial 6, in which the SW detected the environment segments more than one time, are exposed.

By comparing the Tables 4.4 and 4.1 (presented in Section 4.3), it is possible to conclude that the majority of the percentage errors presented in Table 4.4 are lower

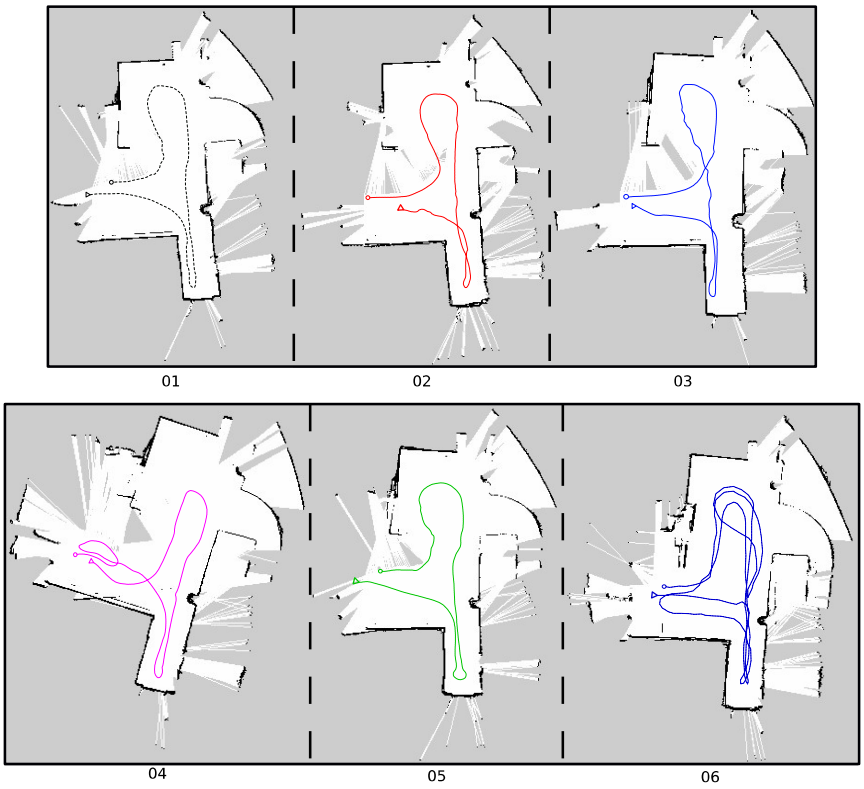


FIGURE 4.6: Generated maps of trials 01 to 06 and SW displacement. Circle means the trials' beginning and the triangle, the end.

TABLE 4.4: Mapping and localization, short paths: results from trials 1 to 5 in real environment

| **Segment** | **Size(m)** | **Trials 1 to 5** | | | **Trial 1** | **Trial 2** | **Trial 3** | **Trial 4** | **Trial 5** |
|---|---|---|---|---|---|---|---|---|---|
| | | $\overline{Size}(m)$ | $\overline{\lvert error \rvert}$ (m) | $\overline{error}$ (%) | Size(m) | Size(m) | Size(m) | Size(m) | Size(m) |
| A | 3.06 | 2.99±0.04 | 0.05±0.04 | 1.63±1.35 | 3.01 | 3.05 | 2.95 | 3.03 | 2.95 |
| B | 2.63 | 2.51±0.14 | 0.08±0.14 | 3.04±5.37 | 2.55 | 2.55 | 2.52 | 2.25 | 2.68 |
| C | 5.59 | 5.57±0.16 | 0.01±0.14 | 0.17±2.62 | 5.6 | 5.65 | 5.55 | 5.75 | 5.31 |
| D | 3.57 | 3.42±0.09 | 0.11±0.09 | 3.08±2.60 | 3.46 | 3.42 | 3.5 | 3.5 | 3.25 |
| E | 1.95 | 1.94±0.03 | 0.00±0.03 | 0.00±1.75 | 1.91 | 1.92 | 1.95 | 1.95 | 2.00 |

than in Table 4.1, except for the segments B and D in which the robot performed a short 90° rotation, which can be considered as a fast movement [95].

The behavior cited in the last paragraph occurs when comparing the Table 4.5 with the 4.2, from Section 4.3, and their percentage error values are almost in the the same range. In both the SW visited all the five segments more than three times.

In order to select the best map to use in the Autonomous Navigation and Obstacles Avoidance validation, we compare the errors between the real segment length

TABLE 4.5: Mapping and localization, long path: results from trial 6

| Segment | Size(m) | Trial 6 | | |
|---|---|---|---|---|
| | | (m) | $\|error\|$ (m) | $error$ (%) |
| A | 3.05 | 2.95 | 0.11 | 3.59 |
| B | 2.63 | 2.68 | 0.05 | 1.90 |
| C | 5.59 | 5.58 | 0.01 | 0.17 |
| D | 3.57 | 3.45 | 0.12 | 3.36 |
| E | 1.95 | 2.0 | 0.05 | 2.56 |

and the estimated of all the trials (Tables 4.4 and 4.5). Finally, we chose the the map generated in the Trial 6 to be used in the next experiments.

### 4.4.2 Autonomous Navigation and obstacle avoidance

The validation of the autonomous navigation strategy was conducted in two parts. In the first one, the SW has to achieve 6 targets, in sequence, and no new obstacles were placed between them, unlike the second sequence which has the presence of three unknown obstacles along the map. The main reason of this approach is to expose and analyze the robot intrinsic errors while performing the developed REI strategy without and with unknown obstacles, and validate if it achieved all the targets without any collision.

The six predefined targets were sent to the SW by using the *path_generator* package and for both sequences, with and without new obstacles, and five trials were conducted. The robot displacement for all trials without unknown obstacles is exposed in Figure 4.7 and, in Table 4.6, the position and orientation errors are exposed.

The linear and angular velocities were limited in 0.25 m/s and $\pm 1$ rad/s respectively, and the *inflation_radius* was 0.7. The controller tolerances for both position distance when the robot achieves a target (*xy_goal_tolerance*) and orientation in yaw/rotation (*yaw_goal_tolerance*) was setup, respectively, in 0.20 m and 0.44 rad $\approx$ 25 degrees.

Given that the linear velocity is limited in 0.25 m/s, the UFES CloudWalker speed is considered safe for an usual pace in elderly without any gait disorder [11], its mean value for all trials was 0.133 $\pm 0.105$ m/s.

In general, the mean values of the position errors were less than the tolerance, 20 cm, for the majority of the targets, expect for Target 6 in which it exceeded the tolerance in 23 mm, this value can be considered small in comparison with the wheels

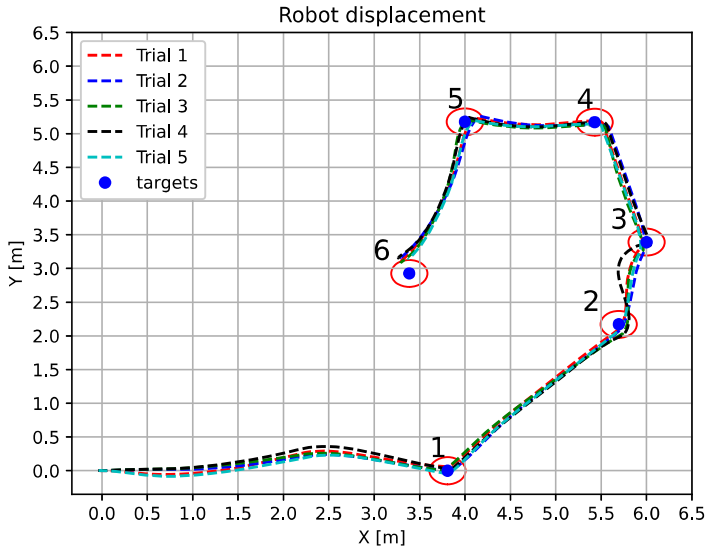


FIGURE 4.7: UFES CloudWalker displacement for all five trials without obstacles in real environment.

TABLE 4.6: Results for Navigation and Obstacles Avoidance with Position (Euclidean distance) and Orientation (angular difference) errors

| Target | Target Pose [x, y, $\theta$] | Robot Pose [$\overline{x}$, $\overline{y}$,$\overline{\theta}$] | Position Error (m) | Orientation Error (rad) |
|---|---|---|---|---|
| 1 | [3.808, 0.000, 0.856] | [3.822±0.030, 0.014±0.036, 0.635±0.061] | 0.020±0.020 | 0.221±0.061 |
| 2 | [5.694, 2.172, 1.4449] | [5.711±0.027, 2.070±0.034, 1.077±0.036] | 0.102±0.037 | 0.367±0.036 |
| 3 | [6.000,3.390, 1.838] | [5.962±0.037, 3.315±0.033, 1.545±0.104] | 0.083±0.030 | 0.293±0.104 |
| 4 | [5.429,5.170, -3.131] | [5.509±0.029, 5.143±0.023, 2.949±0.021] | 0.084±0.028 | 0.182±0.021 |
| 5 | [3.999, 5.176, -2.038] | [4.083±0.046,5.222±0.023, -2.271±0.028] | 0.095±0.045 | 0.233±0.028 |
| 6 | [3.386, 2.926, -1.6313] | [3.295±0.039, 3.130±0.030, -2.049±0.023] | 0.223±0.031 | 0.417±0.023 |

separation distance of the robot, 800 mm. In other hand, all the orientation error values were less than the tolerance (0.44 rad).

Figure 4.8 illustrates the UFES CloudWalker displacement for all the 5 trials in the experiment with three unknown obstacles. There, it is possible to note that the SW reached all the targets without any collisions, meaning that the robot interact with new objects in the environment through the Hokuyo LRF sensor.

The empty red circles around the unknown objects illustrates the effect of the *inflation_radius* parameter influence, used to guarantee that the SW will not collide with them. The targets, SW pose, the Euclidean distance between the destination point and the place where the robot stopped and the orientation error for all trials are presented in Table 4.7.

TABLE 4.7: Results for Navigation and Obstacles Avoidance with Position (Euclidean distance) and Orientation (angular difference) errors

| Target | Target Pose [x, y, $\theta$] | Robot Pose [$\overline{x}, \overline{y}, \overline{\theta}$] | Position Error (m) | Orientation Error (rad) |
|---|---|---|---|---|
| 1 | [3.808, 0.000, 0.856] | [3.811±0.029, -0.023±0.027, 0.618±0.033] | 0.024±0.020 | 0.238±0.033 |
| 2 | [5.694, 2.172, 1.4449] | [5.926±0.188, 2.014±0.070, 1.204±0.101] | 0.280±0.085 | 0.240±0.101 |
| 3 | [6.000,3.390, 1.838] | [6.011±0.054, 3.311±0.057, 1.451±0.091] | 0.079±0.053 | 0.387±0.091 |
| 4 | [5.429,5.170, -3.131] | [5.574±0.058, 5.149±0.025, 2.929±0.026] | 0.146±0.059 | 0.201±0.026 |
| 5 | [3.999, 5.176, -2.038] | [4.096±0.069,5.221±0.024, -2.258±0.048] | 0.106±0.061 | 0.219±0.048 |
| 6 | [3.386, 2.926, -1.6313] | [3.283±0.037, 3.125±0.024, -1.471±0.246] | 0.223±0.019 | 0.160±0.246 |

The mean position error values for the targets 1, 3 , 4 and 5 were less than the tolerance, 20 cm. In target 2, in which the robot local planner modified the previous path to achieve it due a unknown object, this value exceeded the tolerance in 80 mm. The same behaviour happened in the last target, in which this value exceeded the tolerance in 23 mm.

For the majority of the targets the mean value of the robot position error kept less than the tolerance, except for targets 2, in which the robot local planner modified the previous path to achieve this target, and as expected in the last sequence of trials the robot position was higher for target 6. All the orientation errors were less than the tolerance.

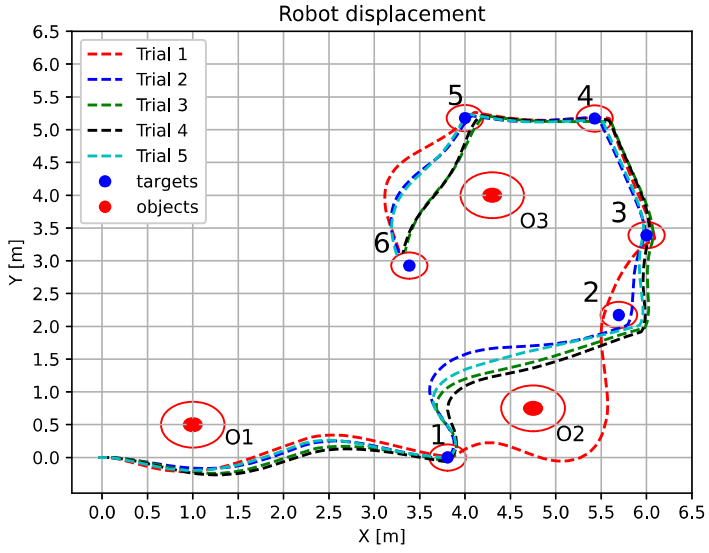


FIGURE 4.8: UFES CloudWalker displacement for all five trials with unknown obstacles in real environment.

Finally, due the fact that the global and local planners are based on probabilistic methods, the robot displacement for trial 1 is different from the others when it avoided the second unknown object.

## 4.5 Preliminary Conclusions

This chapter presented the development and validation of an autonomous navigation strategy applied to the UFES CloudWalker. The mapping and localization experiments in simulation environment proved that despite the errors presented in the Table 4.1, the proposed strategy, through the ROS framework, provided enough evidence about its consistency. In the second experiment, it was proven that the proposed autonomous navigation strategy for known and unknown objects, provided a safety path for a guided lower-limb rehabilitation therapy.

The validation results for the mapping and localization experiment indicate the reliability of the developed setup and algorithm. The combination of both quadrature encoders and IMU data, processed by the *robot_pose_ekf* [16] ROS node in order to estimate a better robot position, provided percentage errors even lower than the exposed in the simulation environment.

From the analysis of the autonomous navigation and obstacles avoidance experiments results, it is possible to infer that this implementation allows the robot to achieve each target successfully. In general, the majority of the errors position errors were smaller than the tolerances, remembering that in the cases when the opposite occurs, the exceeded value was 32 time smaller than the robot wheels separation length.

Once the development of autonomous navigation strategy was validated, the next step is to develop and validate an strategy which will allows shared control between the human, robot and environment. In the next chapter, the development of an HREI control strategy is presented.

[16] http://wiki.ros.org/robot_pose_ekf

# Chapter 5

# Development and Validation of Human-Robot-Environment Interaction Strategy

In this chapter, the Development and Validation of HREI strategy is presented. The motivation of such implementation is to allow the UFES CloudWalker the capacity to provide guided lower limb rehabilitation autonomously respecting the user's needs and the environment constraints. The proposed strategy allows our robotic platform to adjust its velocity while it assists the user's locomotion in the environment.

## 5.1 Materials and Methods

All the experiments conducted in this chapter used the same setup of Section 4.4, the UFES CloudWalker, the autonomous navigation strategy described in it, and the same environment were used. The main difference here is that we use the RPLIDAR A3 LRF sensor to acquire the user's legs data. This sensor was positioned 33.8 cm above the ground with maximum range adjusted to 70 cm and with 60° of FoV from 155° clockwise angle.

The Figure 5.1 is a representation of the UFES CloudWalker top view which summarizes the relationship between the two laser scanner sensors employed, the Hokuyo (readings in dashed blue) is pointed to the environment while the RPLIDAR A3 (readings in dashed red) to the user's legs.

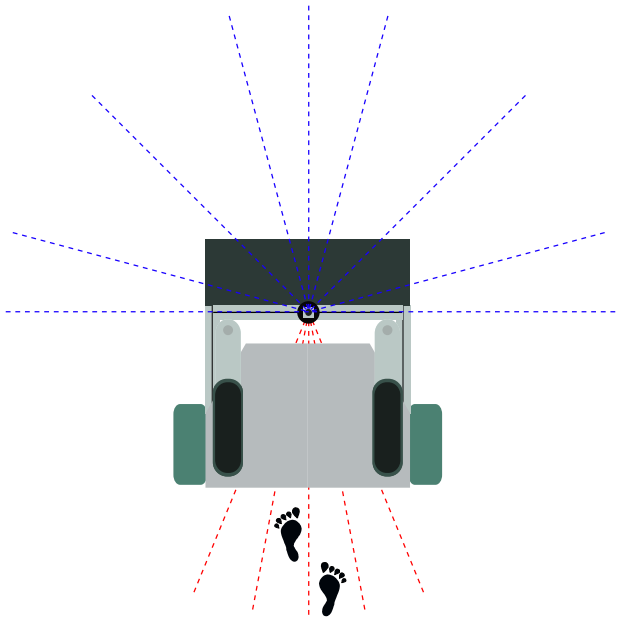

FIGURE 5.1: Relationship between Hokuyo and RPLIDAR A3 laser scanners in top view.

The Leg Detection Module presented in [28] is used to estimate the position of the user's legs and also his distance to the robot through the LRF readings. We create two virtual zones to infer whether the user wants to interact with the robot or not (Figure 5.2).

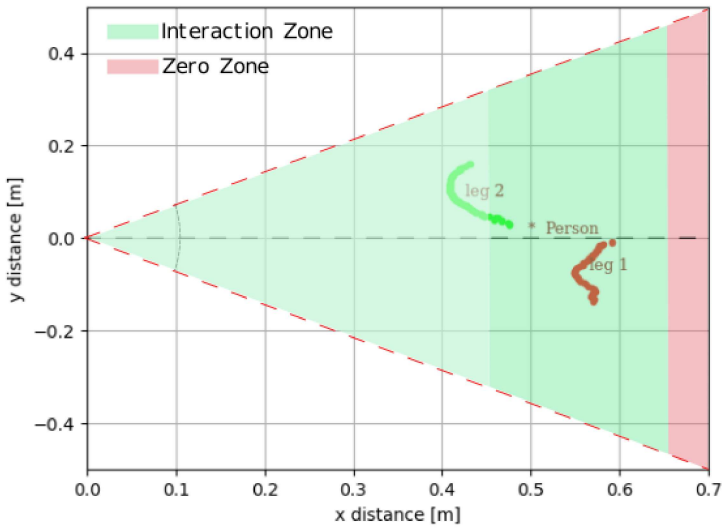


FIGURE 5.2: Interaction and zero zones between the Human and the SW.

The HREI controller, depicted in Figure 5.3, receives two inputs: The estimated distance between the human and the robot, and the velocity command calculated by the REI strategy. The robot only begins to move if the user is inside the Interaction Zone, at least 65 cm of distance.

Distance values between 65 cm and 45 cm influences the previous velocity command calculated by the autonomous navigation strategy and applies a proportional gain, from 0.0 to 1.0, accordingly the Human position. In cases when the user is faster than the SW, distance values smaller than 45 cm, the proportional gain remains at 1.0, and the robot velocity commands will keep at its maximum value, previous calculated in the autonomous navigation module.

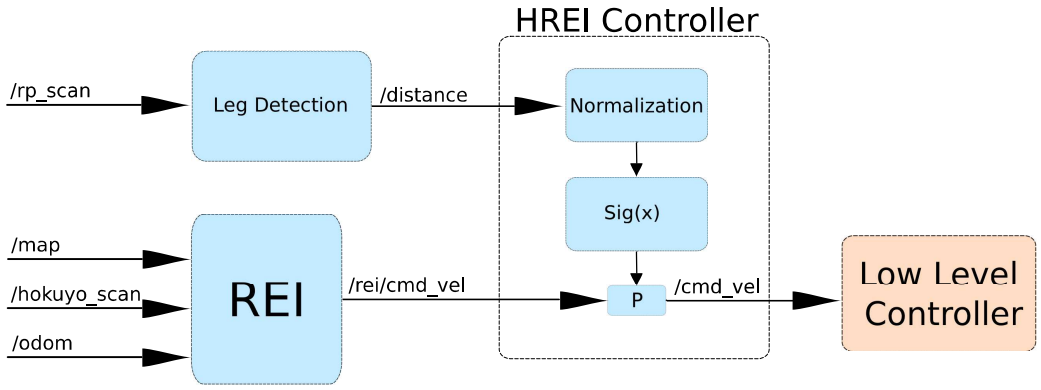


FIGURE 5.3: HREI controller workflow.

When the human is inside the Interaction Zone ($0.45 \leq$ distance $\leq 0.65$), the first step is to change the distance value by simply calculation of the subtraction absolute value between beginning of the interaction zone and the actual distance, $d$ accordingly Equation 5.1. The $D_{zone}$ could result in values from 0.0 to 0.20.

$$D_{zone}(k) = |0.65 - d(k)| \tag{5.1}$$

Once the $D_{zone}$ was calculated, the next process is to normalize it from 0.0 to 1.0. After this, it is possible to calculate the Proportional Gain through a modified Sigmoid function, Equation 5.2, with $\beta$ equals to 2 and $x$ is an alias to $D_{zone}$. The behaviour of such implementation is depicted in Figure 5.4.

$$P(k) = \frac{1}{1 + (\frac{x(k)}{1-x(k)})^{-\beta}} \tag{5.2}$$

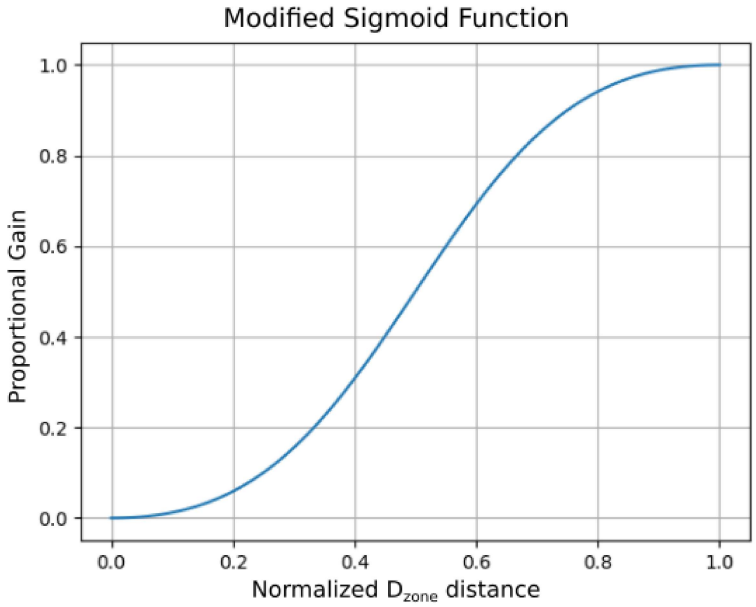


FIGURE 5.4: Modified Sigmoid function which calculates the Proportional Gain.

The last steps are to apply the Proportional Gain in both linear and angular velocity previously calculated by the REI strategy, respectively Equations 5.3 and 5.4, and send it to the Low Level Controller through the */cmd_vel* ROS topic.

$$\text{New Linear Velocity} : V_{HREI}(k) = P(k) \times V_{REI} \tag{5.3}$$

$$\text{New Angular Velocity} : \omega_{HREI}(k) = P(k) \times \omega_{REI} \tag{5.4}$$

The experimental procedures follow the same methodology adopted in subsection 4.4.2: two scenarios were conducted. In the first one, five health individuals (three women and two men, average height: 1.72 m) were asked to be assisted by the UFES CloudWalker, while it was achieving target by target. At this point, we were interested to validate the performance of our new controller, which takes into account the user position, in the guided locomotion task between each target. No unknown objects were placed in the environment.

In the last scenario, we asked to only one individual, a woman with 1.65 m of height, to stop anytime while the robot assists her, simulating a possible fatigue or fail. Two unknown objects were also placed in the environment during the experiment. In this case, we were trying to investigate no only if the robot achieved all

the targets, but also if it was respecting the user's needs and the changes in the environment. Results for both sequences were exposed in the next section.

## 5.2 Results and Discussion

The results for the first 5 trials with healthy individuals and no unknown obstacles in the environment are exposed bellow. Table 5.1 shows the position and orientation errors when the SW reaches each target, and Figure 5.5 the robot displacement for all the five trials.

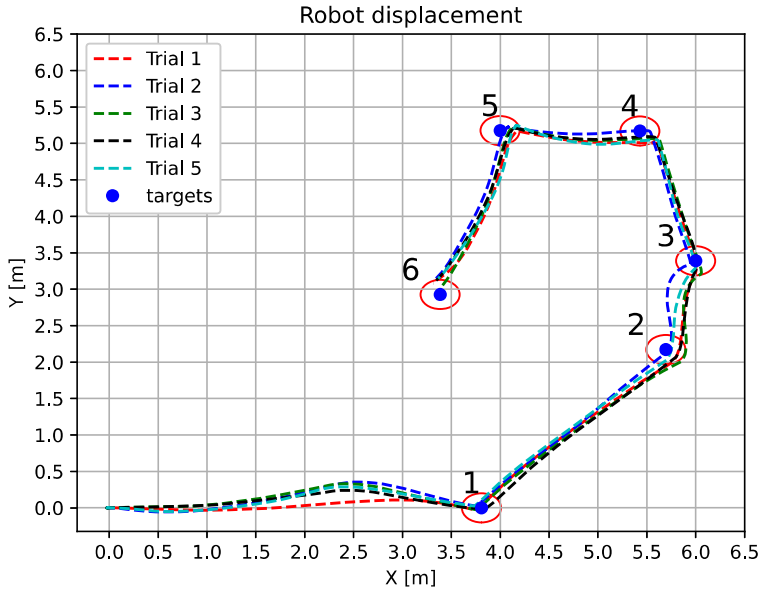


FIGURE 5.5: UFES CloudWalker displacement for all five trials with no obstacles in the environment.

By observation of Figure 5.5 it is possible to infer that the SW behaviour was similar to the depicted in Figure 4.7. In Table 5.1, the mean values of the position errors for targets 1,2,3,5 and 6 were less than the tolerance, 20 cm, only for target 4 this value exceeded the tolerance in 1 mm. All the orientation errors were less than the tolerance, 0.44 rad, except for target 6 in which this value exceeded the tolerance in 0.015 rad. Almost all the orientation errors were less than the tolerance. Only in Trial 6 it was observed that this value exceeded the tolerance in 0.015 radians.

Figure 5.6 illustrates the robot displacement in the environment with unknown obstacles being positioned while the SW is guiding the human to the targets. The

TABLE 5.1: Results for validation of the HREI strategy with Position (Euclidean distance) and Orientation (angular difference) errors

| Target | Target Pose [x, y, $\theta$] | Robot Pose [$\overline{x}, \overline{y}, \overline{\theta}$] | Position Error (m) | Orientation Error (rad) |
|---|---|---|---|---|
| 1 | [3.808, 0.000, 0.856] | [3.760±0.042, -0.010±0.027, 0.681±0.050] | 0.049±0.024 | 0.175±0.050 |
| 2 | [5.694, 2.172, 1.4449] | [5.772±0.065, 2.055±0.045, 1.085±0.033] | 0.141±0.066 | 0.360±0.033 |
| 3 | [6.000,3.390, 1.838] | [6.001±0.033, 3.277±0.048, 1.514±0.087] | 0.113±0.044 | 0.325±0.087 |
| 4 | [5.429,5.170, -3.131] | [5.606±0.036, 5.074±0.053, -2.9770.037] | 0.201±0.050 | 0.154±0.037 |
| 5 | [3.999, 5.176, -2.038] | [4.146±0.043,5.211±0.029, -2.203±0.037] | 0.150±0.040 | 0.165±0.037 |
| 6 | [3.386, 2.926, -1.6313] | [3.362±0.045, 3.098±0.044, -2.086±0.036] | 0.173±0.046 | 0.455±0.036 |

position and orientation errors of this experiment are detailed in Table 5.2. It is observed that for targets 2, 3, 4 and 5 the mean values of the position errors were higher than the tolerance.

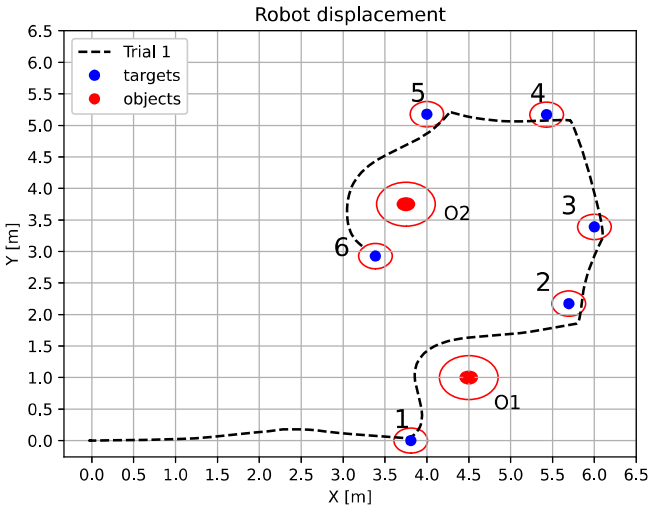


FIGURE 5.6: UFES CloudWalker displacement for the last trial, in which unknown obstacles were placed in the environment.

To understand these results, it is important to analyze the autonomous navigation strategy commands, the influence of the human's legs distance in the proposed HREI strategy commands and how the UFES CloudWalker performed in respect to these commands. Figure 5.7 presents the human's distance from our robot during the trial and the its relationship with the proportional gain.

We use the red rectangles to highlight the segments in which the user stops to walk, simulating fall or fatigue. In the blue ones, we shown those in which the user's velocity was higher than that of our SW.

TABLE 5.2: Results for Navigation and Obstacles Avoidance with Position (Euclidean distance) and Orientation (angular difference) errors

| Target | Target Pose [x, y, $\theta$] | Robot Pose [x, y, $\theta$] | Position Error (m) | Orientation Error (rad) |
|---|---|---|---|---|
| 1 | [3.808, 0.000, 0.856] | [3.790,0.040, 0.599] | 0.043 | 0.258 |
| 2 | [5.694, 2.172, 1.4449] | [5.801, 1.861, 1.156] | 0.328 | 0.289 |
| 3 | [6.000,3.390, 1.838] | [6.095, 3.206, 1.421] | 0.207 | 0.418 |
| 4 | [5.429,5.170, -3.131] | [5.712, 5.076, -2.934] | 0.298 | 0.198 |
| 5 | [3.999, 5.176, -2.038] | [4.275,5.207, -2.211] | 0.277 | 0.172 |
| 6 | [3.386, 2.926, -1.6313] | [3.253, 3.056, -1.576] | 0.186 | 0.055 |

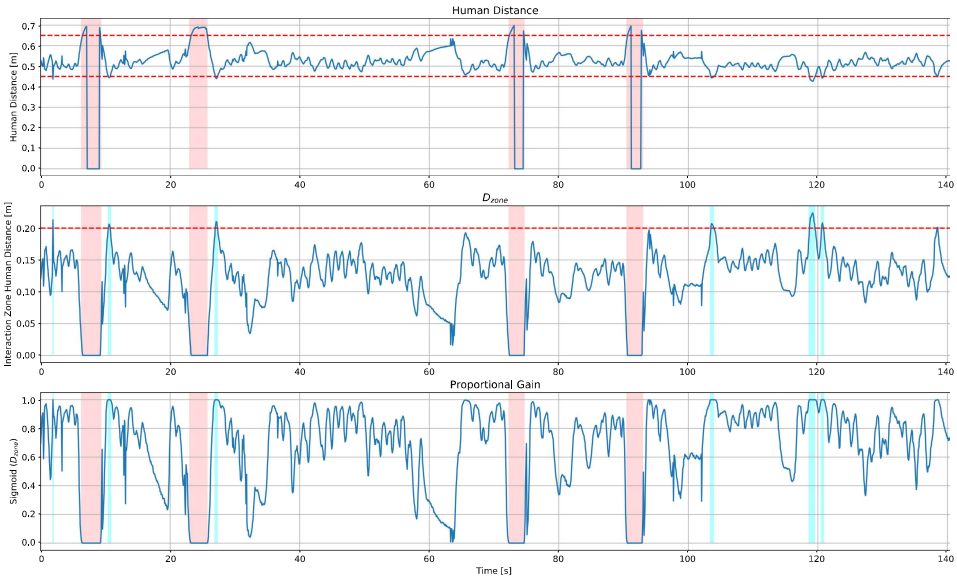


FIGURE 5.7: From top to bottom: the Human Distance, The $D_{zone}$ value and the Proportional Gain.

In the three graphics in Figure 5.8 we present the linear and angular velocities commands from both autonomous navigation and HREI strategies, and also the UFES CloudWalker performance. We used yellow rectangles to show the segments in which the SW position is closer the target, and the red ones to present again the influence of the proportional gain in both HREI velocity commands and , consecutively, the UFES CloudWalker performance.

Due the unknown obstacle positioned when the robot achieved the target 1 (Figure 5.6) it performed a fast turn to left, positive angular velocity value in Figure 5.8, consecutively the position error was higher than the others in target 2, an excess of

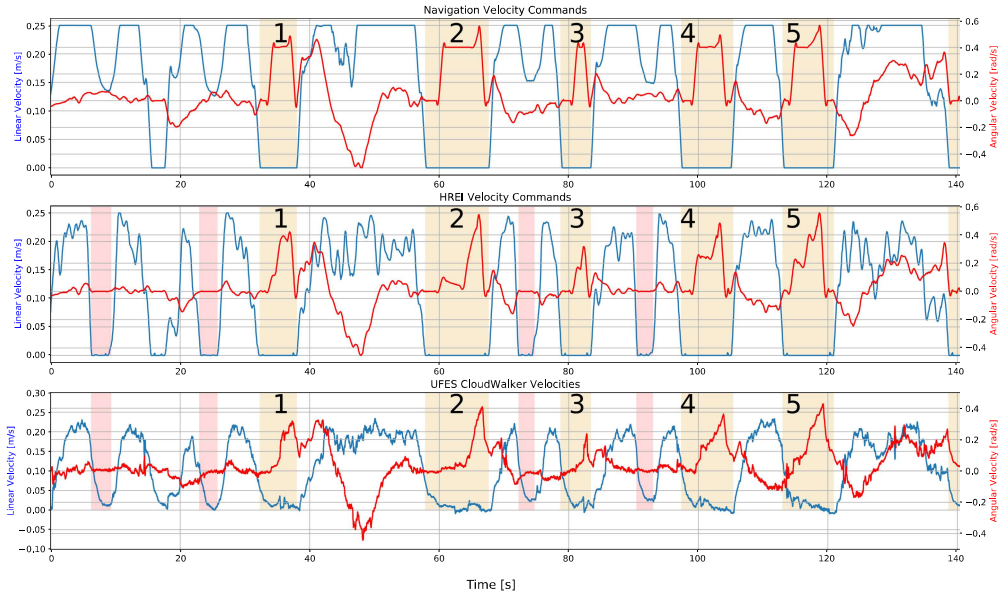


FIGURE 5.8: Velocity commands and robot odometry: REI, HREI and odometry.

128 mm in the tolerance value. In target 3, the position error also exceed the tolerance in 7 mm.

Between targets 3 and 4 the user made a pause which forced the SW to stop, proportional gain equals to zero. After this, she returns to walk and the robot began to guide her. This break and walk results in an position error 98 mm above the tolerance in Target 4 and probably Target 5.

The maximum excess values in the position errors, 128 mm in target 2, is six times smaller than the robot wheels distance, 800 mm. Ultimately, all the orientation errors were less than the tolerance.

## 5.3 Preliminary conclusions

In this Chapter, the development and validation of a Human Robot Environment Interaction strategy through both Autonomous Navigation and obstacle avoidance algorithm, and the user's leg distance applied in the Smart Walker was conducted.

For the first trials sequence, no unknown obstacles, it is possible to affirm that the robot performance was similar to the experiments in subsection 4.4.2. Although the control has been shared among human, robot and the autonomous navigation strategy, the robot reached each trial with success while guiding the human.

When changes in the environment were done, the UFES CloudWalker detected and avoided collisions with them. There's no collisions between the robot and new obstacles. Our SW stops instantly when the user made pauses, avoiding falls and respecting possible user's fatigue. Although it was observed some excesses in the position errors, it is possible to affirm that the UFES CloudWalker adapts its behaviour accordingly the user and the changes in the environment while providing guidance in the task to achieve each target of the six predefined targets.

# Chapter 6

# Conclusion and Future Work

Mobility is the most relevant physical ability that impacts directly people's life, whether in individual activities or in group. In Chapter 1, we described our motivation to write this master's thesis, our research group expertise with smart walkers, as well as, the current trends reported in the literature about this topic. Then, in Chapter 2, we presented a theoretical background in mobility assistive devices, focusing in smart walkers, and ultimately the concept of cloud robotics with some examples of applications in healthcare.

We shown, in Chapter 3, an overview of the proposed robotic platform, the UFES CloudWalker and details related to the development of its hardware and software architectures, and the integration with its subsystems for HREI strategies.

Chapter 4, illustrates the process of development of a REI control strategy in simulation and real environments. The results in simulation environment proved the reliability of the proposed implementation and all the errors from both mapping and autonomous navigation indicated the necessity of refine the robot pose through an IMU.

In real environment, several challenges were found and solved, from the design of the hardware and integration with all the sensors, to time synchronization between robot and remote PC. We also improved the estimation of the robot pose through the Extended Kalman Filter.

Finally, in Chapter 5 an HREI control strategy was developed and validated. The HREI controller mixed data from the autonomous navigation strategy cited in Chapter 4 and the user's distance from the SW. This strategy allowed the robot to adapt its behaviour accordingly the environment changes and the user necessities.

Due this, the robotic platform stopped moving when the human made pauses and also avoided collision with new obstacles placed in the environment while it was guiding him.

After the conclusion of this work, several possibilities for the future are viable. Once the validation of the experiments were conducted in local network and the processing was made in a notebook, the exploitation of such approaches can be integrated with a VM stored on the cloud.

The developed autonomous navigation strategy creates paths in which the robot only fixes the orientation error when the position error to the target is smaller. This can be considered dangerous to a lower limb disability person due the movement of rotation under itself. Due this, a new improvement must be done in the path planners to avoid this movement creating paths in which the robot will reach the target with the desired rotation or closer it.

In this dissertation, no user experience analysis was conducted. In the future, it is important to elaborate experimental protocols to measure both qualitative and quantitative data related to the users' experience.

Ultimately, the experiments were conducted in health people which was useful to validate the proposed HREI strategy. As a future work, long-term experiments in rehabilitation clinics could be conducted aiming to evaluate the patients rehabilitation progress with such robotic device.

# Bibliography


[1] U. Nations, D. of Economic, S. Affairs, and P. Division, "World Population Prospects 2019 Highlights," Tech. Rep.

[2] L. Ferrucci, R. Cooper, M. Shardell, E. M. Simonsick, J. A. Schrack, and D. Kuh, *Age-related change in mobility: Perspectives from life course epidemiology and geroscience*, 2016. DOI: 10.1093/gerona/glw043.

[3] M. N. B. Nguyen, Z. Hasnain, M. Li, T. Dorff, D. Quinn, S. Purushotham, L. Nocera, P. K. Newton, P. Kuhn, J. Nieva, and C. Shahabi, "Mining human mobility to quantify performance status," in *2017 IEEE International Conference on Data Mining Workshops (ICDMW)*, 2017, pp. 1172–1177. DOI: 10.1109/ICDMW.2017.168.

[4] C. Lott and M. J. Johnson, "Upper limb kinematics of adults with cerebral palsy on bilateral functional tasks," in *Proceedings of the Annual International Conference of the IEEE Engineering in Medicine and Biology Society, EMBS*, vol. 2016-October, Institute of Electrical and Electronics Engineers Inc., 2016, pp. 5676–5679, ISBN: 9781457702204. DOI: 10.1109/EMBC.2016.7592015.

[5] K. M. Nordin, K. Chellappan, and R. Sahathevan, "Upper limb rehabilitation in post stroke patients: Clinical observation," in *IECBES 2014, Conference Proceedings - 2014 IEEE Conference on Biomedical Engineering and Sciences: "Miri, Where Engineering in Medicine and Biology and Humanity Meet"*, Institute of Electrical and Electronics Engineers Inc., 2014, pp. 700–704, ISBN: 9781479940844. DOI: 10.1109/IECBES.2014.7047597.

[6] J. C. Singer and G. Mochizuki, "Post-stroke lower limb spasticity alters the interlimb temporal synchronization of centre of pressure displacements across multiple timescales," *IEEE Transactions on Neural Systems and Rehabilitation Engineering*, vol. 23, no. 5, pp. 786–795, 2015, ISSN: 15344320. DOI: 10.1109/TNSRE.2014.2353636.

[7] F. Yakub, A. Z. M. Khudzari, and Y. Mori, "Recent trends for practical rehabilitation robotics, current challenges and the future," *International Journal of*

*Rehabilitation Research*, vol. 37, no. 1, pp. 9–21, Mar. 2014. DOI: 10.1097/mrr.0000000000000035. [Online]. Available: https://doi.org/10.1097/mrr.0000000000000035.

[8] M. L. Toro-Hernández, P. Kankipati, M. Goldberg, S. Contepomi, D. R. Tsukimoto, and N. Bray, "Appropriate assistive technology for developing countries," *Physical Medicine and Rehabilitation Clinics of North America*, vol. 30, no. 4, pp. 847–865, Nov. 2019. DOI: 10.1016/j.pmr.2019.07.008. [Online]. Available: https://doi.org/10.1016/j.pmr.2019.07.008.

[9] A. Mancisidor, A. Zubizarreta, I. Cabanes, P. Bengoa, and J. H. Jung, *New Trends in Medical and Service Robots*. 2018, ISBN: 978-3-319-59971-7. DOI: 10.1007/978-3-319-59972-4.

[10] O. N. Berdina, T. A. Bairova, L. V. Rychkova, and S. A. Sheptunov, "The pediatric robotic-assisted rehabilitation complex for children and adolescents with cerebral palsy: Background and product design," in *Proceedings of the 2017 International Conference "Quality Management, Transport and Information Security, Information Technologies", IT and QM and IS 2017*, Institute of Electrical and Electronics Engineers Inc., 2017, pp. 360–363, ISBN: 9781538607039. DOI: 10.1109/ITMQIS.2017.8085834.

[11] "Assistive locomotion device with haptic feedback for guiding visually impaired people," *Medical Engineering Physics*, 2020, ISSN: 1350-4533. DOI: https://doi.org/10.1016/j.medengphy.2020.04.002.

[12] P. Beckerle, G. Salvietti, R. Unal, D. Prattichizzo, S. Rossi, C. Castellini, S. Hirche, S. Endo, H. B. Amor, M. Ciocarlie, F. Mastrogiovanni, B. D. Argall, and M. Bianchi, *A human-robot interaction perspective on assistive and rehabilitation robotics*, 2017. DOI: 10.3389/fnbot.2017.00024.

[13] T. B. Sheridan, *Human-Robot Interaction*, 4. SAGE Publications Inc., 2016, vol. 58, pp. 525–532. DOI: 10.1177/0018720816644364.

[14] A. Malviya and R. Kala, "Social robot motion planning using contextual distances observed from 3d human motion tracking," *Expert Systems with Applications*, vol. 184, p. 115 515, 2021, ISSN: 0957-4174. DOI: https://doi.org/10.1016/j.eswa.2021.115515. [Online]. Available: https://www.sciencedirect.com/science/article/pii/S0957417421009258.

[15] M. F. J. Hernández, "Human-robot-environment interaction strategies for walker-assisted gait," available in: http://repositorio.ufes.br/handle/10/10923, Ph.D. dissertation, Federal University of Espírito Santo, Dec. 2018.

[16] G. Toffetti, T. Lötscher, S. Kenzhegulov, J. Spillner, and T. M. Bohnert, "Cloud robotics: SLAM and autonomous exploration on PaaS," in *UCC 2017 Companion - Companion Proceedings of the 10th International Conference on Utility and Cloud Computing*, 2017, ISBN: 9781450351959. DOI: 10.1145/3147234.3148100.

[17] V. A. S. Júnior, "Detecção de pernas utilizando um sensor de varredura laser aplicada a um andador robótico," M.S. thesis, Federal University of Espírito Santo, Brazil, Vitória-ES, 2013.

[18] C. A. R. Díaz, "Estratégia de Apoio à marcha humana assistida por andador robótico baseada em forças de interação," M.S. thesis, Federal University of Espírito Santo, Brazil, Vitória-ES, 2014.

[19] C. A. Cifuentes, C Rodriguez, A Frizera-Neto, T. F. Bastos-Filho, and R Carelli, "Multimodal Human–Robot Interaction for Walker-Assisted Gait," *IEEE Systems Journal*, vol. 10, no. 3, pp. 933–943, 2016, ISSN: 1932-8184. DOI: 10.1109/JSYST.2014.2318698.

[20] M. F. Jiménez, M. Monllor, A. Frizera, T. Bastos, F. Roberti, and R. Carelli, "Admittance Controller with Spatial Modulation for Assisted Locomotion using a Smart Walker," *Journal of Intelligent & Robotic Systems*, 2018, ISSN: 1573-0409. DOI: 10.1007/s10846-018-0854-0.

[21] M. F. Jiménez, W. Scheidegger, R. C. Mello, T. Bastos, and A. Frizera, "Bringing proxemics to walker-assisted gait: Using admittance control with spatial modulation to navigate in confined spaces," *Personal and Ubiquitous Computing*, Mar. 2021. DOI: 10.1007/s00779-021-01521-8. [Online]. Available: https://doi.org/10.1007/s00779-021-01521-8.

[22] A. G. Leal-Junior, C. R. Diaz, M. F. Jimenez, C. Leitao, C. Marques, M. J. Pontes, and A. Frizera, "Polymer optical fiber-based sensor system for smart walker instrumentation and health assessment," vol. 19, no. 2, pp. 567–574, Jan. 2019. DOI: 10.1109/jsen.2018.2878735. [Online]. Available: https://doi.org/10.1109/jsen.2018.2878735.

[23] A. G. Leal-Junior, A. Frizera, A. Theodosiou, C. Diaz, M. Jimenez, R. Min, M. J. Pontes, K. Kalli, and C. Marques, "Plane-by-plane written, low-loss polymer optical fiber bragg grating arrays for multiparameter sensing in a smart walker," vol. 19, no. 20, pp. 9221–9228, Oct. 2019. DOI: 10.1109/jsen.2019.2921419. [Online]. Available: https://doi.org/10.1109/jsen.2019.2921419.

[24] R. Mello, M. Jimenez, F. Souza, M. R. N. Ribeiro, and A. Frizera-Neto, "Towards a new generation of smart devices for mobility assistance: CloudWalker, a cloud-enabled cyber-physical system," in *2018 7th IEEE International Conference on Biomedical Robotics and Biomechatronics (Biorob)*, IEEE, Aug. 2018. DOI: 10.1109/biorob.2018.8488077. [Online]. Available: https://doi.org/10.1109/biorob.2018.8488077.

[25] R. C. de Mello, M. F. Jimenez, M. R. N. Ribeiro, R. L. Guimarães, and A. Frizera-Neto, "On human-in-the-loop CPS in healthcare: A cloud-enabled mobility assistance service," *Robotica*, vol. 37, no. 9, pp. 1477–1493, Feb. 2019. DOI: 10.1017/s0263574719000079. [Online]. Available: https://doi.org/10.1017/s0263574719000079.

[26] R. C. Mello, S. D. Sierra, M. Múnera, C. A. Cifuentes, M. R. N. Ribeiro, and A. Frizera-Neto, "Cloud robotics experimentation testbeds: A cloud-based navigation case study," in *2019 IEEE 4th Colombian Conference on Automatic Control (CCAC)*, 2019, pp. 1–6.

[27] W. M. Scheidegger, R. C. De Mello, S. D. Sierra, M. F. Jimenez, M. C. Munera, C. A. Cifuentes, and A. Frizera-Neto, "A novel multimodal cognitive interaction for walker-assisted rehabilitation therapies," in *IEEE International Conference on Rehabilitation Robotics*, 2019, ISBN: 9781728127552. DOI: 10.1109/ICORR.2019.8779469.

[28] W. M. Scheidegger, R. C. de Mello, S. D. Sierra M., M. F. Jimenez, M. C. Múnera, C. A. Cifuentes, and A. Frizera-Neto, "A novel multimodal cognitive interaction for walker-assisted rehabilitation therapies," in *2019 IEEE 16th International Conference on Rehabilitation Robotics (ICORR)*, 2019, pp. 905–910.

[29] K. Charalampous, I. Kostavelis, and A. Gasteratos, "Robot navigation in large-scale social maps: An action recognition approach," *Expert Systems with Applications*, vol. 66, pp. 261–273, 2016, ISSN: 0957-4174. DOI: https://doi.org/10.1016/j.eswa.2016.09.026. [Online]. Available: https://www.sciencedirect.com/science/article/pii/S0957417416305103.

[30] M. Munaro and E. Menegatti, "Fast RGB-d people tracking for service robots," 3, vol. 37, Springer Science and Business Media LLC, Feb. 2014, pp. 227–242. DOI: 10.1007/s10514-014-9385-0. [Online]. Available: https://doi.org/10.1007/s10514-014-9385-0.

[31] A. Wachaja, P. Agarwal, M. Zink, M. R. Adame, K. Moller, and W. Burgard, "Navigating blind people with a smart walker," IEEE, Sep. 2015. DOI: 10.

1109/iros.2015.7354233. [Online]. Available: https://doi.org/10.1109/iros.2015.7354233.

[32] A. Wachaja, P. Agarwal, M. Zink, M. R. Adame, K. Möller, and W. Burgard, "Navigating blind people with walking impairments using a smart walker," *Autonomous Robots*, vol. 41, no. 3, pp. 555–573, 2017, ISSN: 15737527. DOI: 10.1007/s10514-016-9595-8.

[33] G. Moustris, N. Kardaris, A. Tsiami, G. Chalvatzaki, P. Koutras, A. Dometios, P. Oikonomou, C. Tzafestas, P. Maragos, E. Efthimiou, X. Papageorgiou, S.-E. Fotinea, Y. Koumpouros, A. Vacalopoulou, E. Papageorgiou, A. Karavasili, F. Koureta, D. Dimou, A. Nikolakakis, K. Karaiskos, and P. Mavridis, "The i-walk lightweight assistive rollator: First evaluation study," *Frontiers in Robotics and AI*, vol. 8, p. 272, 2021, ISSN: 2296-9144. DOI: 10.3389/frobt.2021.677542. [Online]. Available: https://www.frontiersin.org/article/10.3389/frobt.2021.677542.

[34] L. Palopoli, A. Argyros, J. Birchbauer, A. Colombo, D. Fontanelli, A. Legay, A. Garulli, A. Giannitrapani, D. Macii, F. Moro, P. Nazemzadeh, P. Padeleris, R. Passerone, G. Poier, D. Prattichizzo, T. Rizano, L. Rizzon, S. Scheggi, and S. Sedwards, "Navigation assistance and guidance of older adults across complex public spaces: The DALi approach," vol. 8, no. 2, pp. 77–92, Mar. 2015. DOI: 10.1007/s11370-015-0169-y. [Online]. Available: https://doi.org/10.1007/s11370-015-0169-y.

[35] X. Zhao, Z. Zhu, M. Liu, C. Zhao, Y. Zhao, J. Pan, Z. Wang, and C. Wu, "A smart robotic walker with intelligent close-proximity interaction capabilities for elderly mobility safety," *Frontiers in Neurorobotics*, vol. 14, p. 75, 2020, ISSN: 1662-5218. DOI: 10.3389/fnbot.2020.575889. [Online]. Available: https://www.frontiersin.org/article/10.3389/fnbot.2020.575889.

[36] J. Ballesteros, C. Urdiales, A. B. Martinez, and M. Tirado, "Automatic assessment of a rollator-user's condition during rehabilitation using the i-walker platform," vol. 25, no. 11, pp. 2009–2017, Nov. 2017. DOI: 10.1109/tnsre.2017.2698005. [Online]. Available: https://doi.org/10.1109/tnsre.2017.2698005.

[37] G. Morone, R. Annicchiarico, M. Iosa, A. Federici, S. Paolucci, U. Cortés, and C. Caltagirone, "Overground walking training with the i-walker, a robotic servo-assistive device, enhances balance in patients with subacute stroke: A randomized controlled trial," vol. 13, no. 1, May 2016. DOI: 10.1186/s12984-

016-0155-4. [Online]. Available: https://doi.org/10.1186/s12984-016-0155-4.

[38] J. Ballesteros, C. Urdiales, A. B. Martinez, and M. Tirado, "Automatic assessment of a rollator-user's condition during rehabilitation using the i-walker platform," vol. 25, no. 11, pp. 2009–2017, Nov. 2017. DOI: 10.1109/tnsre.2017.2698005. [Online]. Available: https://doi.org/10.1109/tnsre.2017.2698005.

[39] J. Paulo, P. Peixoto, and U. J. Nunes, "ISR-AIWALKER: Robotic walker for intuitive and safe mobility assistance and gait analysis," vol. 47, no. 6, pp. 1110–1122, Dec. 2017. DOI: 10.1109/thms.2017.2759807. [Online]. Available: https://doi.org/10.1109/thms.2017.2759807.

[40] L. Garrote, J. Paulo, J. Perdiz, P. Peixoto, and U. J. Nunes, "Robot-assisted navigation for a robotic walker with aided user intent," IEEE, Aug. 2018. DOI: 10.1109/roman.2018.8525674. [Online]. Available: https://doi.org/10.1109/roman.2018.8525674.

[41] L. Garrote, J. Paulo, and U. J. Nunes, "Reinforcement learning aided robot-assisted navigation: A utility and RRT two-stage approach," vol. 12, no. 3, pp. 689–707, Sep. 2019. DOI: 10.1007/s12369-019-00585-0. [Online]. Available: https://doi.org/10.1007/s12369-019-00585-0.

[42] X. S. Papageorgiou, G. Chalvatzaki, K.-N. Lianos, C. Werner, K. Hauer, C. S. Tzafestas, and P. Maragos, "Experimental validation of human pathological gait analysis for an assisted living intelligent robotic walker," IEEE, Jun. 2016. DOI: 10.1109/biorob.2016.7523776. [Online]. Available: https://doi.org/10.1109/biorob.2016.7523776.

[43] E. Efthimiou, S.-E. Fotinea, T. Goulas, M. Koutsombogera, P. Karioris, A. Vacalopoulou, I. Rodomagoulakis, P. Maragos, C. Tzafestas, V. Pitsikalis, Y. Koumpouros, A. Karavasili, P. Siavelis, F. Koureta, and D. Alexopoulou, "The MOBOT rollator human-robot interaction model and user evaluation process," IEEE, Dec. 2016. DOI: 10.1109/ssci.2016.7850061. [Online]. Available: https://doi.org/10.1109/ssci.2016.7850061.

[44] E. Efthimiou, S.-E. Fotinea, T. Goulas, A.-L. Dimou, M. Koutsombogera, V. Pitsikalis, P. Maragos, and C. Tzafestas, "The mobot platform – showcasing multimodality in human-assistive robot interaction," in *Universal Access in*

*Human-Computer Interaction. Interaction Techniques and Environments*, M. Antona and C. Stephanidis, Eds., Cham: Springer International Publishing, 2016, pp. 382–391, ISBN: 978-3-319-40244-4.

[45] R. Moreira, J. Alves, A. Matias, and C. Santos, "Smart and assistive walker – ASBGo: Rehabilitation robotics: A smart–walker to assist ataxic patients," in, Springer International Publishing, 2019, pp. 37–68. DOI: 10.1007/978-3-030-24230-5_2. [Online]. Available: https://doi.org/10.1007/978-3-030-24230-5_2.

[46] J. Alves, E. Seabra, I. Caetano, and C. P. Santos, "Overview of the asbgo++ smart walker," in *2017 IEEE 5th Portuguese Meeting on Bioengineering (ENBENG)*, 2017, pp. 1–4. DOI: 10.1109/ENBENG.2017.7889420.

[47] I. Caetano, J. Alves, J. Goncalves, M. Martins, and C. P. Santos, "Development of a biofeedback approach using body tracking with active depth sensor in ASBGo smart walker," IEEE, May 2016. DOI: 10.1109/icarsc.2016.34. [Online]. Available: https://doi.org/10.1109/icarsc.2016.34.

[48] M. Palermo, S. Moccia, L. Migliorelli, E. Frontoni, and C. P. Santos, "Real-time human pose estimation on a smart walker using convolutional neural networks," vol. 184, p. 115 498, Dec. 2021. DOI: 10.1016/j.eswa.2021.115498. [Online]. Available: https://doi.org/10.1016/j.eswa.2021.115498.

[49] C. Bayon, O. Ramirez, M. D. Del Castillo, J. I. Serrano, R. Raya, J. M. Belda-Lois, R. Poveda, F. Molla, T. Martin, I. Martinez, S. Lerma Lara, and E. Rocon, in *Proceedings - IEEE International Conference on Robotics and Automation*. DOI: 10.1109/ICRA.2016.7487561.

[50] C. A. Cifuentes, C. Bayon, S. Lerma, A. Frizera, and E. Rocon, "Human-robot interaction strategy for overground rehabilitation in patients with cerebral palsy," IEEE, Jun. 2016. DOI: 10.1109/biorob.2016.7523713. [Online]. Available: https://doi.org/10.1109/biorob.2016.7523713.

[51] L. F. Aycardi, C. A. Cifuentes, M. Múnera, C. Bayón, O. Ramírez, S. Lerma, A. Frizera, and E. Rocon, "Evaluation of biomechanical gait parameters of patients with Cerebral Palsy at three different levels of gait assistance using the CPWalker," *Journal of NeuroEngineering and Rehabilitation*, 2019, ISSN: 17430003. DOI: 10.1186/s12984-019-0485-0.

[52] S. D. S. Sierra M., M. Garzón, M. Múnera, and C. A. Cifuentes, "Human–Robot–Environment Interaction Interface for Smart Walker Assisted Gait: AGoRA Walker," *Sensors*, 2019, ISSN: 1424-8220. DOI: 10.3390/s19132897.

[53] S. D. S. M, M. Múnera, T. Provot, M. Bourgain, and C. A. Cifuentes, "Evaluation of physical interaction during walker-assisted gait with the AGoRA walker: Strategies based on virtual mechanical stiffness," *Sensors*, vol. 21, no. 9, p. 3242, May 2021. DOI: 10.3390/s21093242. [Online]. Available: https://doi.org/10.3390/s21093242.

[54] J. Simanek, M. Reinstein, and V. Kubelka, "Evaluation of the ekf-based estimation architectures for data fusion in mobile robots," *IEEE/ASME Transactions on Mechatronics*, vol. 20, no. 2, pp. 985–990, 2015.

[55] D. Helbing and P. Molnár, "Social force model for pedestrian dynamics," vol. 51, no. 5, pp. 4282–4286, May 1995. DOI: 10.1103/physreve.51.4282. [Online]. Available: https://doi.org/10.1103/physreve.51.4282.

[56] G. Grisetti, C. Stachniss, and W. Burgard, "Improved techniques for grid mapping with rao-blackwellized particle filters," *IEEE Transactions on Robotics*, vol. 23, no. 1, pp. 34–46, 2007. DOI: 10.1109/TRO.2006.889486.

[57] F. W. Van Hook, D. Demonbreun, and B. D. Weiss, "Ambulatory devices for chronic gait disorders in the elderly," en, *Am. Fam. Physician*, vol. 67, no. 8, pp. 1717–1724, Apr. 2003.

[58] A. Prabhakar, S Indulakshmi, M Jeyaram, A. R Stalin, G. Kasthuri, and P. Ramanathan, "Making assistive devices affordable," in *TENCON 2019 - 2019 IEEE Region 10 Conference (TENCON)*, IEEE, Oct. 2019. DOI: 10.1109/tencon.2019.8929591. [Online]. Available: https://doi.org/10.1109/tencon.2019.8929591.

[59] M. M. Martins, C. P. Santos, A. Frizera-Neto, and R. Ceres, "Assistive mobility devices focusing on smart walkers: Classification and review," *Robotics and Autonomous Systems*, vol. 60, no. 4, pp. 548–562, 2012, ISSN: 0921-8890. DOI: https://doi.org/10.1016/j.robot.2011.11.015.

[60] A. Frizera-Neto, R. Ceres, E. Rocon, and J. L. Pons, "Empowering and assisting natural human mobility: The simbiosis walker," *International Journal of Advanced Robotic Systems*, 2011, ISSN: 17298814. DOI: 10.5772/10666.

[61] S. Stowe, J. Hopes, and G. Mulley, "Gerotechnology series: 2. walking aids," *European Geriatric Medicine*, vol. 1, no. 2, pp. 122–127, 2010, ISSN: 1878-7649. DOI: https://doi.org/10.1016/j.eurger.2010.02.003.

[62] O. Postolache, J. M. Dias Pereira, V. Viegas, L. Pedro, P. S. Girao, R. Oliveira, and G. Postolache, "Smart walker solutions for physical rehabilitation," *IEEE Instrumentation Measurement Magazine*, vol. 18, no. 5, pp. 21–30, 2015. DOI: 10.1109/MIM.2015.7271223.

[63] C. Werner, P. Ullrich, M. Geravand, A. Peer, J. M. Bauer, and K. Hauer, "A systematic review of study results reported for the evaluation of robotic rollators from the perspective of users," *Disability and Rehabilitation: Assistive Technology*, vol. 13, no. 1, pp. 31–39, 2018, PMID: 28125298. DOI: 10.1080/17483107.2016.1278470.

[64] G. J. Lacey and D. Rodriguez-Losada, "The evolution of guido," vol. 15, no. 4, pp. 75–83, Dec. 2008. DOI: 10.1109/mra.2008.929924. [Online]. Available: https://doi.org/10.1109/mra.2008.929924.

[65] M. Spenko, H. Yu, and S. Dubowsky, "Robotic personal aids for mobility and monitoring for the elderly," *IEEE Transactions on Neural Systems and Rehabilitation Engineering*, vol. 14, no. 3, pp. 344–351, 2006. DOI: 10.1109/TNSRE.2006.881534.

[66] J. S. Henry and V. Aharonson, "Gait monitoring for the elderly using a robotic walking aid," IEEE, Nov. 2010. DOI: 10.1109/eeei.2010.5662196. [Online]. Available: https://doi.org/10.1109/eeei.2010.5662196.

[67] G. Lee, T. Ohnuma, and N. Y. Chong, "Design and control of JAIST active robotic walker," *Intelligent Service Robotics*, vol. 3, no. 3, pp. 125–135, Apr. 2010. DOI: 10.1007/s11370-010-0064-5. [Online]. Available: https://doi.org/10.1007/s11370-010-0064-5.

[68] A. F. Neto, J. A. Gallego, E. Rocon, J. L. Pons, and R. Ceres, "Extraction of user's navigation commands from upper body force interaction in walker assisted gait," vol. 9, no. 1, Aug. 2010. DOI: 10.1186/1475-925x-9-37. [Online]. Available: https://doi.org/10.1186/1475-925x-9-37.

[69] M. Chang, W. Mou, C. Liao, and L. Fu, "Design and implementation of an active robotic walker for parkinson's patients," in *2012 Proceedings of SICE Annual Conference (SICE)*, 2012, pp. 2068–2073.

[70] R. Meattini, S. Benatti, U. Scarcia, D. De Gregorio, L. Benini, and C. Melchiorri, "An semg-based human–robot interface for robotic hands using machine learning and synergies," *IEEE Transactions on Components, Packaging and Manufacturing Technology*, vol. 8, no. 7, pp. 1149–1158, 2018. DOI: 10.1109/TCPMT.2018.2799987.

[71] N. Céspedes, D. Raigoso, M. Múnera, and C. A. Cifuentes, "Long-term social human-robot interaction for neurorehabilitation: Robots as a tool to support gait therapy in the pandemic," *Frontiers in Neurorobotics*, vol. 15, Feb. 2021. DOI: 10.3389/fnbot.2021.612034. [Online]. Available: https://doi.org/10.3389/fnbot.2021.612034.

[72] J. L. Pons, *Wearable Robots: Biomechatronic Exoskeletons*. NJ: Wiley-Blackwell, Mar. 2008.

[73] J. Ye, G. Chen, Q. Liu, L. Duan, W. Shang, X. Yao, J. Long, Y. Wang, Z. Wu, and C. Wang, "An adaptive shared control of a novel robotic walker for gait rehabilitation of stroke patients," in *2018 IEEE International Conference on Intelligence and Safety for Robotics (ISR)*, IEEE, Aug. 2018. DOI: 10.1109/iisr.2018.8535892. [Online]. Available: https://doi.org/10.1109/iisr.2018.8535892.

[74] M. Daza, D. Barrios-Aranibar, J. Diaz-Amado, Y. Cardinale, and J. Vilasboas, "An approach of social navigation based on proxemics for crowded environments of humans and robots," *Micromachines*, vol. 12, no. 2, p. 193, Feb. 2021. DOI: 10.3390/mi12020193. [Online]. Available: https://doi.org/10.3390/mi12020193.

[75] C Nandhini, A. Murmu, and R. Doriya, "Study and analysis of cloud-based robotics framework," in *2017 International Conference on Current Trends in Computer, Electrical, Electronics and Communication (CTCEEC)*, IEEE, Sep. 2017. DOI: 10.1109/ctceec.2017.8455104. [Online]. Available: https://doi.org/10.1109/ctceec.2017.8455104.

[76] Q. Zhang, L. Cheng, and R. Boutaba, "Cloud computing: State-of-the-art and research challenges," *Journal of Internet Services and Applications*, vol. 1, no. 1, pp. 7–18, Apr. 2010. DOI: 10.1007/s13174-010-0007-6. [Online]. Available: https://doi.org/10.1007/s13174-010-0007-6.

[77] V. Kumar and R. S. Rathore, "Security issues with virtualization in cloud computing," in *2018 International Conference on Advances in Computing, Communication Control and Networking (ICACCCN)*, IEEE, Oct. 2018. DOI: 10.1109/icacccn.2018.8748405. [Online]. Available: https://doi.org/10.1109/icacccn.2018.8748405.

[78] K. Kamei, S. Nishio, N. Hagita, and M. Sato, "Cloud networked robotics," *IEEE Network*, vol. 26, no. 3, pp. 28–34, May 2012. DOI: 10.1109/mnet.

2012.6201213. [Online]. Available: https://doi.org/10.1109/mnet.2012.6201213.

[79] S. A. Miratabzadeh, N. Gallardo, N. Gamez, K. Haradi, A. R. Puthussery, P. Rad, and M. Jamshidi, "Cloud robotics: A software architecture: For heterogeneous large-scale autonomous robots," in *2016 World Automation Congress (WAC)*, IEEE, Jul. 2016. DOI: 10.1109/wac.2016.7583017. [Online]. Available: https://doi.org/10.1109/wac.2016.7583017.

[80] M. Bonaccorsi, L. Fiorini, F. Cavallo, A. Saffiotti, and P. Dario, "A cloud robotics solution to improve social assistive robots for active and healthy aging," *International Journal of Social Robotics*, vol. 8, no. 3, pp. 393–408, May 2016. DOI: 10.1007/s12369-016-0351-1. [Online]. Available: https://doi.org/10.1007/s12369-016-0351-1.

[81] L. Fiorini, R. Esposito, M. Bonaccorsi, C. Petrazzuolo, F. Saponara, R. Giannantonio, G. D. Petris, P. Dario, and F. Cavallo, "Enabling personalised medical support for chronic disease management through a hybrid robot-cloud approach," *Autonomous Robots*, vol. 41, no. 5, pp. 1263–1276, Jul. 2016. DOI: 10.1007/s10514-016-9586-9. [Online]. Available: https://doi.org/10.1007/s10514-016-9586-9.

[82] C. Radu, C. Candea, and G. Candea, "Towards an assistive system for human," in *Proceedings of the 9th ACM International Conference on PErvasive Technologies Related to Assistive Environments*, ACM, Jun. 2016. DOI: 10.1145/2910674.2910677. [Online]. Available: https://doi.org/10.1145/2910674.2910677.

[83] H. Zhang and L. Zhang, "Cloud robotics architecture: Trends and challenges," in *2019 IEEE International Conference on Service-Oriented System Engineering (SOSE)*, IEEE, Apr. 2019. DOI: 10.1109/sose.2019.00061. [Online]. Available: https://doi.org/10.1109/sose.2019.00061.

[84] N. K. Beigi, B. Partov, and S. Farokhi, "Real-time cloud robotics in practical smart city applications," in *2017 IEEE 28th Annual International Symposium on Personal, Indoor, and Mobile Radio Communications (PIMRC)*, IEEE, Oct. 2017. DOI: 10.1109/pimrc.2017.8292655. [Online]. Available: https://doi.org/10.1109/pimrc.2017.8292655.

[85] R. C. Mello, M. F. Jimenez, M. R. N. Ribeiro, R. Laiola Guimaraes, and A. Frizera-Neto, DOI: 10.1017/S0263574719000079.

[86] YoonSeok, HanCheol, RyuWoon, and TaeHoon, *ROS Robot Programming*. ROBOTIS Co.,Ltd, 2017, ISBN: 979-11-962307-1-5.

[87] M. Faisal, M. Alsulaiman, R. Hedjar, H. Mathkour, M. Zuair, H. Altaheri, M. Zakariah, M. A. Bencherif, and M. A. Mekhtiche, "Enhancement of mobile robot localization using extended kalman filter," *Advances in Mechanical Engineering*, vol. 8, no. 11, p. 168 781 401 668 014, Nov. 2016. DOI: 10.1177/1687814016680142. [Online]. Available: https://doi.org/10.1177/1687814016680142.

[88] T. Nam, J. Shim, and Y. Cho, "A 2.5d map-based mobile robot localization via cooperation of aerial and ground robots," *Sensors*, vol. 17, no. 12, p. 2730, Nov. 2017. DOI: 10.3390/s17122730. [Online]. Available: https://doi.org/10.3390/s17122730.

[89] F. Dellaert, D. Fox, W. Burgard, and S. Thrun, "Monte carlo localization for mobile robots," in *Proceedings 1999 IEEE International Conference on Robotics and Automation (Cat. No.99CH36288C)*, IEEE. DOI: 10.1109/robot.1999.772544. [Online]. Available: https://doi.org/10.1109/robot.1999.772544.

[90] E. W. Dijkstra, "A note on two problems in connexion with graphs," *Numerische mathematik*, vol. 1, no. 1, pp. 269–271, 1959.

[91] D. Fox, W. Burgard, and S. Thrun, "The dynamic window approach to collision avoidance," *IEEE Robotics and Automation Magazine*, 1997, ISSN: 10709932. DOI: 10.1109/100.580977.

[92] J. Shi and Tomasi, "Good features to track," in *Proceedings of IEEE Conference on Computer Vision and Pattern Recognition CVPR-94*, IEEE Comput. Soc. Press, 1994. DOI: 10.1109/cvpr.1994.323794. [Online]. Available: https://doi.org/10.1109/cvpr.1994.323794.

[93] Y. Abdelrasoul, A. B. S. H. Saman, and P. Sebastian, "A quantitative study of tuning ROS gmapping parameters and their effect on performing indoor 2d SLAM," in *2016 2nd IEEE International Symposium on Robotics and Manufacturing Automation (ROMA)*, IEEE, Sep. 2016. DOI: 10.1109/roma.2016.7847825. [Online]. Available: https://doi.org/10.1109/roma.2016.7847825.

[94] R. E. Kalman, "A new approach to linear filtering and prediction problems," *Journal of Basic Engineering*, vol. 82, no. 1, pp. 35–45, Mar. 1960. DOI: 10.

1115/1.3662552. [Online]. Available: https://doi.org/10.1115/1.3662552.

[95] M. Filipenko and I. Afanasyev, "Comparison of Various SLAM Systems for Mobile Robot in an Indoor Environment," in *9th International Conference on Intelligent Systems 2018: Theory, Research and Innovation in Applications, IS 2018 - Proceedings*, 2018, ISBN: 9781538670972. DOI: 10.1109/IS.2018.8710464.

# Appendix A

# Low Level Controller

The low level control loop receives as input velocity commands from the Walker_-PC which could be generated by the user or control strategies which publishes messages directly in the */cmd_vel* topic. Two independent PID controllers are used in this implementation (Figure A.1).

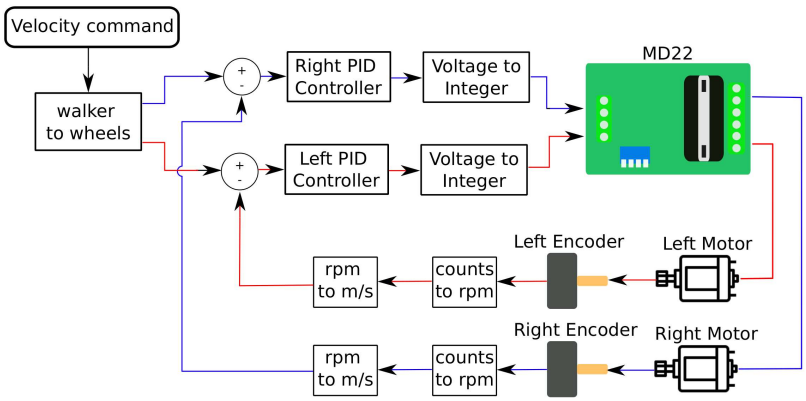


FIGURE A.1: The UFES CloudWalker low level control unity in which the red lines represent right wheel control loop and the blue, the left.

From the velocity command is possible to extract both linear ($V$) and angular ($w$) velocities, respectively *msg.linear.x* and *msg.angular.z*. They are used in the block *walker to wheels* which calculates both left ($V_{left}$) and right ($V_{right}$) reference velocities in m/s accordingly Equations A.1 and A.2. The $d$ means wheels separation distance.

$$V_{left} = V - \frac{w \times d}{2} \tag{A.1}$$

$$V_{right} = V + \frac{w \times d}{2} \tag{A.2}$$

We leverage the counts from quadrature encoders coupled in both left and right motors to get their rotation speed in rpm through Equation A.3, in which $\Delta P$ means pulses counts variation, $PPR$ is for Pulses Per Revolution, $GR$ the Gear Ratio and $\Delta T$ is the time time elapsed between each acquisition loop. To convert the velocities from each wheel from rpm to in m/s we use the *rpm to m/s* block. The only parameter to be setup is the wheel radius, $R$, accordingly Equation A.4.

$$V_{rpm} = \frac{\Delta P}{PPR} \times \frac{1.0}{GR} \times \frac{60.0}{\Delta T} \tag{A.3}$$

$$V_{m/s} = \frac{2 \times \pi \times R}{60.0} \times V_{rpm} \tag{A.4}$$

Once we have both reference and current signal, the error is calculated and sent to individual PID controllers which calculates the respective voltage signal that will be converted to a 8-bit integer value ($I$),Equation A.5, and sent to the MD22 driver.

$$I = V_{PID} \times 5.3125 + 127.5 \tag{A.5}$$

We use also the wheels velocities in m/s to calculate the robot odometry. Linear ($V$) and angular ($w$) velocities are calculate accordingly Equations A.6 and A.7. The walker pose $[x, y, \theta]$ estimation from the wheels encoders is calculate accordingly Equations A.8, A.9 and A.10.

$$V = \frac{V_{left} + V_{right}}{2} \tag{A.6}$$

$$w = \frac{V_{right} - V_{left}}{d} \tag{A.7}$$

$$x(k) = x(k-1) + V(k) \times cos(\theta(k)) \times (t(k) - t(k-1)) \tag{A.8}$$

$$y(k) = y(k-1) + V \times sin(\theta(k)) \times (t(k) - t(k-1)) \tag{A.9}$$

$$\theta(k) = \theta(k-1) + w(k) \times (t(k) - t(k-1)) \tag{A.10}$$